DETERMINATION OF GUIDANCE LAWS FOR UAV SYSTEMS IN COMMUNICATION NETWORKS USING COLLISION CONE THEORY

by
UTSAV MUDGAL

THESIS

Submitted in Partial fulfillment of the requirements
for the degree of Master of Science at
The University of Texas at Arlington
December 2021

Arlington, TX

Supervising Committee:

Chakravarthy, Animesh; Supervising Professor
Wang, Shuo Linda
Bowling, Alan

ACKNOWLEDGMENTS

First and foremost, I would like to acknowledge the contribution of Dr. Animesh Chakravarthy, for his guidance, and support throughout the development of this thesis. From guidance in courses to application of studies done in class towards this thesis, he had some of the most insightful and thought-provoking methods to inspiring a young mind. It has truly been an honor to have had the opportunity to work on my thesis under his guidance and to have been able to call him my mentor.

Further I am grateful to Dr David A Hullender, for introducing me to the world of controls and inspiring me to take a deeper dive into the field. Your contribution to pacing me into the field and introducing aspects of modeling and simulation made the completion of this work much simpler.

I would also like to thank the Mechanical and Aerospace Engineering department at the University of Texas at Arlington, with special mention to Dr. Shuo Linda Wang and Dr. Alan Bowling for being a part of my thesis committee.

Furthermore, I'd like to mention to Pranay Gadiya and Ruchir Chug, thank you for keeping me on track and making me stick to a schedule and all the people who have contributed to shaping the last two years soaked in academia, joy, and peace. It has truly been one of the greatest two years of my life.

DEDICATION

I dedicate this thesis to my lovely family and friends, those that I received and those whom I found. I want to take this opportunity to thank my lovely parents, Papa, you have been courageous and went above and beyond to ensure I had excellent education. Ma, I am forever in your debt, you made me into the person that I am today, you have had the greatest impact on me, as a human and as an engineer, everything that I am is because of your efforts and patience.

I am extremely grateful to my uncles & aunts who have never let me feel that I have been living on the other side of the globe for the last two years. They have taken me in and have been my idols, my guides, and my cheer during this journey.

A big thank you to all my friends, these two and a half years would not have been the same without them. Shivam Dwivedi, Prajakta Jagtap and everyone who made the struggle worthwhile.

Lastly but certainly not the least, I would like to forward my sincerest gratitude to Shilpa Ganesh More. Her contribution towards this work and being my greatest cheerleader is something which is beyond what words can capture. Thank you for being a part of my life.

LIST OF FIGURES

List of Tables

ABSTRACT

DETERMINATION OF GUIDANCE LAWS FOR UAV SYSTEMS IN COMMUNICATION NETWORKS USING COLLISION CONE THEORY

UTSAV MUDGAL, M.S.
AEROSPACE ENGINEERING

The University of Texas at Arlington,2021

Supervising Professor: Animesh Chakravarthy

Unmanned Aerial Vehicles (UAVs), also commonly known as drones, are used in various applications, including military applications such as surveillance and intelligence-gathering as well as civilian applications such as search and rescue. The use of UAVs to form communication networks is a topic of active research interest. This thesis aims to investigate the development of guidance laws for multiple UAVs to form such communication networks. Toward this end, this thesis employs tools from collision cone theory and incorporates them with parameters used to describe a communication network. Different types of networks are evaluated for use of the guidance laws. Simulation results are presented for various scenarios.

TABLE OF CONTENTS

Chapter 1 Introduction

1.1 Motivation

UAVs, commonly known as drones have seen an increase in usage across the spectrum in recent years. Applications range from military operations, police surveillance, intelligence and many more. UAVs have also found application in media such as movies, television, and internet-based media platforms. Many web-based influencers have now furthered how they develop content with the application of UAV mounted camera systems. With the development of autonomous flight modes in UAVs it is further apparent that application spaces for UAVs are bound to become more abundant in the near future.

Currently the field of telecommunications is rapidly expanding at a speed much higher than ever in the past. 88.5% of the United States population was online in 2018 as compared to only 9.24% in 1995 [1] and the number of mobile phone subscriptions have increased from 12.74 connections for every 100 people to 134.46 connections for every 100 people during the same time. Furthermore, we have also seen the time spent with digital media increase from under 3 hours in 2008 to over 6 hours in 2018, where we also see an increase in the percentage share for digital data consumed on mobile phones.

Internet and data transfer speeds have seen a major upgrade in the past few years. While the email has been around since the 1960's and TCP/IP settings were standardized in 1982. The development of Wi-Fi and high frequency communication setups such as 5G and Wi-Fi 5 has introduced certain challenges when it comes to maintaining stronger connections between base stations and end users. These communication modes tend to have very high

frequency but travel through shorter distance that they can travel due to the wave form that the radio frequencies work on. Simply put the higher the frequency, the lower the distance that the wave can travel.

Access points (APs) can be used for increasing the range of high frequency communication as is apparent in the use of Wi-Fi 5 in households or neighborhoods with public 5.0 GHz Wi-Fi. These devices act as relays to enhance the coverage area for communication networks. However, these do come with their own drawbacks, such as physical installation and changing the connection patterns based on where the user and base station are in relation to each other.

The UAVs can provide dynamic access points for communication networks in remote locations and sparsely populated suburban areas. We can also employ these UAVs in leader follower pattern to increase the communication distance to which a single base station can transfer data in certain modes of communication.This represents a motivation to employ UAVs as nodes in communication networks.

1.2 Literature Survey

Communication networks can be understood to work based on a variety of factors, including the power of the transmitter, the gain of the transmission station and the gain value of the receiving station. These play an essential part in the strength of a connection between the transmitter and receiver.

A determining metric which signifies the strength of the connection is SNR or the signal to noise ratio. The signal to noise ratio is a logarithmic ratio of the signal strength to the amount of noise which is entangled in the signal wave.

The uses of VANET and MANET as models to create nodes in ad-hoc networks can be used for development of a system. Some similarities encourage researchers to explore the applicability of the work done for Mobile Ad hoc Networks (MANETs) and Vehicular Ad hoc Networks (VANETs) but works in these areas do not fully address the unique characteristics of UAV networks.

While MANETs and VANETs can provide good means of creating a network, UAVs can act and work in situations that would not be possible with ground level vehicles. For example, UAV networks can be deployed to act as relays and communication centers in disaster struck areas.

In [2] researchers have mentioned various patterns of deploying UAVs for communication networks. In this thesis we would ourselves with the development of the guidance laws for the trajectory that a UAV would take to maintain connect and communication within the system.

Usage of UAVs to develop communication networks is an area of research that has not been extensively researched in the past for civilian purposes and developments in the field are relatively recent. In [6] major contributions in how the positioning and power control of UAVs can be done simultaneously. The paper employs successive convex approximation (SCA) along with fast iterative shrinkage thresholding algorithm (FISTA) type accelerated gradient

projection. The paper elaborates the positioning problem and handles cases of single and multiple user equipment. The basis for the system is for air-to-ground (A2G) communications with assumption of line of sight (LOS) communication. The paper delves deep into the positioning and how the setup of the network can be used to enhance the communication network in the area, and tackles this as an optimization problem for the position of the UAV.

Different researchers in [7], [8], [9], [10], [11] have provided analysis of A2G communication and have dealt with the positioning problem of UAVs in different ways. The problem is mostly dealt in the form of a positional optimization problem.

In this thesis, we deal the problem from a guidance law perspective, to guide a UAV towards a circle of influence that is created due to the power transmission when configuring for different networks such as Wi-Fi and cellular networks.

Guidance for interception and rendezvous of objects can be done by various methods, such as conventional proportional navigation (PN) and generalized guidance laws [3].The authors in [4] have worked on the development of collision cone theory foe obstacle avoidance.

The research community is utilizing the concept of shapes and predictive algorithms for collision avoidance with the help of collision cones. For example, Coppola et al. in their 2018 paper [5] have developed collision avoidance systems based on the onboard communication to provide relative localization of UAVs. The application of collision cone in the paper is used for the avoidance of obstacles in the path of moving agents within a specified area.

A method to use to calculate and employ the trajectory for a UAV to act as relay for communication is rendezvous cones [24], rendezvous cone is a concept based on the collision cone theory. We can utilize the relative position and velocity of various objects in 2D, and 3D space and determine guidance laws that create conditions for a rendezvous among the objects.

Researchers in [24] have shown that this theory can be applied to various objects which could be circular, elliptical, or arbitrarily shaped and have extensively shown conditions for rendezvous between such objects.In this thesis we employ the rendezvous cone approach to develop, guidance laws for UAVs to form communication networks.

1.3 Thesis Organization

This thesis is organized as follows. In chapter 2 we look at the ways UAVs are used in communication networks, and the performance metrics involved in these networks. Chapter 3 shows development of collision cones and how they are used here for the development of guidance laws for motion planning of UAVs. In chapter 4 we demonstrate simulation results for different cases of networks. Finally, in chapter 5 we present conclusions and suggestions for future.

Chapter 2 Wireless Communication Networks

The chapter begins with a short history of the communication network and the development in this field. We then examine the metrics and parameters used to describe a network. We then proceed to highlight the different effects that various parameters have on the communication network and how these effect the influence area that is created by the network. Lastly, the chapter shows various examples of the changes in circle of influence.

2.1 A History of Communication Networks

Communication networks have been in use since the invention of telephone in the late 1800s. Within a couple of decades Guglielmo Marconi had developed a wireless telegraph system based on radio technology. From those early days of transmitting morse code on radio waves till today, the field of wireless communication has developed to a phenomenal extent. [12]

As is presented in [13], one of the first mobile phones was introduced to the world by Martin Cooper, an engineer at Motorola during the 1970s, and one of the first usage of this system was in car phones. Towards the end of the decade, Nippon Telephone and Telegraph Company developed the first generation of mobile phone networks in 1979. By the early 1980s itself the tech gained traction and was popular in Finland, US, UK, and Europe. Based on analog signals the system could work on an 800 MHz to 900 MHz band and was a primitive look into wireless tech when compared to today's networks.

2G communication brought with it to the world, GSM, and CDMA systems. This system boosted the way we could communicate and made it possible for text messaging to become a reality. 2.5G and 2.75G gave us the possibility to incorporate data transfer in terms of "Enhanced

General Packet Radio Service (GPRS-EDGE)", and other capabilities which were hence introduced into communication networks. This was the beginning of access to the internet on our cell phones.

3G started with the introduction of UMTS- Universal Mobile Terrestrial/ Telecommunication Systems. UMTS had a data rate capacity of 384kbps and now made possible to have video calling available to us. Smartphone development saw a huge leap, and specific applications were made for them. 3.5G and 3.75G took this to a step further and introduced HSDPA – High Speed Downlink Packet access and HSUPA – High Speed Uplink Packet Access. 3.5G could now support up to 2 Mbps data rate.

3.9G (also known as long term evolution or LTE) was an even powerful evolvement of the 3G system. 4G network was developed by IEEE, offering data transfer rates up to 1Gbps. Simultaneous transmission of voice and data is possible with LTE system, which greatly improves the data rate. All services including voice services can be transmitted over IP packets.

5G technology as we see today provides data transfer rates up to 10Gbps. 5G is using millimeter wavelength to transmit data.Details about the system and how the range of communication are affected by this will be discussed subsequently.

2.2 Evaluating a Wireless Network

A defining characteristic of the mobile wireless channel is the variation in channel strength over time and over frequency. The variations can be roughly divided into two types:

- *Large-scale fading*, arising from path loss of signal as a function of distance and shadowing by large objects such as buildings and hills.
- *Small-scale fading*, resulting from the constructive and destructive interference of the multiple signal paths between the transmitter and receiver.

When considering a signal in a network one of the ways to quantify it is the use of the Signal-to-Noise-Ratio (SNR) of the signal received at the receiver. Determining the SNR would allow the quantification of the operating distance for which any transmitting and receiving antenna pair would be able to work. When considering radio waves, assuming line of sight communication radio waves can travel up to a horizon distance as shown in Figure below. [14]

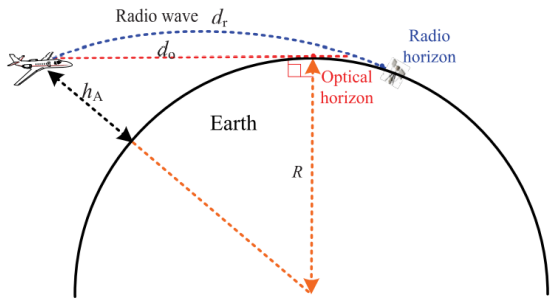

Figure 1 Radio Horizon Distance [14]

The figure depicts the radio horizon distance. If we consider the movement of radio waves through line of sight (LOS) between the transmitter and receiver, then the radio waves can carry information even further than the optical horizon of the wave.

When calculating the SNR value that can possibly be obtained at a distance from the transmitter, large-scale and small-scale fading have effects on the communication area between a transceiver pair. Small-scale fading can also be affected by the wave reflection for the communication channel.

Also, whether the communication occurs in a free space, or a restrictive space, the temperature of the surroundings and various other factors creates different parameters in the formulation of large-scale fading. As this chapter proceeds, these parameters are taken into consideration when calculating the communication area application of the guidance law.

2.2.1 Noise Floor and SNR Calculation

To calculate the amount of SNR, which would allow us to measure the strength of a network, CISCO in their online document [15] have explained the different SNR values that are required to establish a strong connection between a transmitter and receiver set. As mentioned earlier the SNR value is a logarithmic ratio of the power of signal and the noise that is carried within an RF transmission.

Ref. [15] also mentions the ways that the SNR values are established. As shown in Figure 2, the SNR value is based on the noisefloor value. Noise floor is an important reference which helps in the determination of the SNR value in different conditions. Thus, as is shown in the figure, it can be inferred that the SNR value represents the difference between the received signal and the noisefloor value.

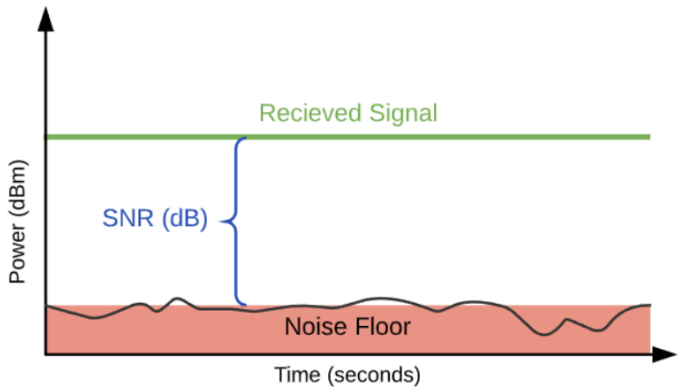

Figure 2 SNR Value Representation [15]

This also creates the situation wherein same value of power as is delivered by the Transmitted /Received Signal would not always deliver the same SNR value in different conditions.

Noise floor can be described as the "level of the minimum signal that can be received" [16]. Since signal noise is an ever-present phenomenon in radio communication it becomes crucial in the determination of the SNR values for a transceiver set.

When keeping the receiver as the only consideration, the value of the noise floor becomes dependent on a variety of factors, one of the primary influencers in this is the minimum input noise at the receiver. This can be calculated using the formula:

$$P = kTB \qquad (2.1)$$

Where:

P is the power in watts

k is the Boltzmann's constant ($1.38 \times 10^{23}\ J/K$)

B is the bandwidth in Hertz

Equation (2.1) can then be used to determine the noise floor value for a particular temperature of a system. For example, at room temperature for a 5G network working at a bandwidth of 100MHz, we would see a noise floor value of -123.85 db.

Furthermore, noise figure is a variation that the system shows due to various factors, a general factor for noise figure when working in a transmitter and receiver pair is 30dB, this is due to the losses incurred due to the antenna.

The formula could also be modified to work based off the variation in bandwidth at $20^{o}C$ as:

$$Noise\ floor = -174\ + Noise\ Figure + 10\log_{10}(Bandwidth) \qquad (2.2)$$

Thus, when calculating the value of the noise floor to facilitate the calculation of the SNR we would have to know the value of the bandwidth. Discussion of the bandwidth values of various networks and power value from cellphones and other devices is presented in the next section.

2.2.2 Bandwidth Capacity for Networks

To calculate the noise floor value, a consideration is the bandwidth of the network that is being used as is mentioned in equations (2.1) and (2.2).

Various networks work in different bandwidth for the frequencies that these networks use. FAA has in the recent past opened frequency bands for operation of 5G networks. Determining the bandwidth in a network is vital for measuring the channels and interference that they may cause.

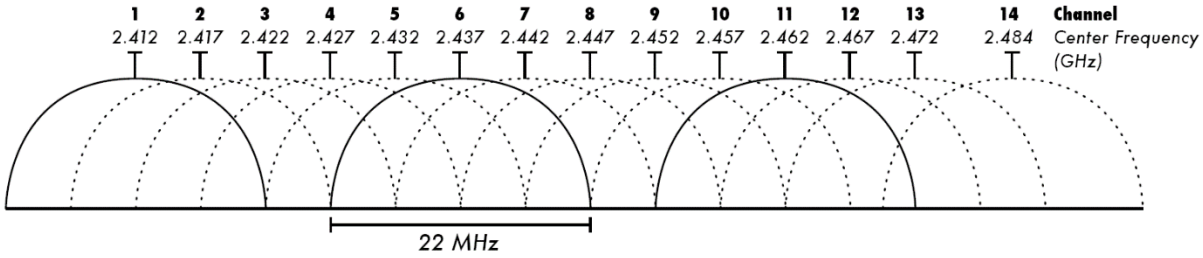

Figure 3 Channels and Center frequencies for 802.11b [17]

Shown above in Figure 3 is the variation in the channels for a Wi-Fi of 802.11b (Wi-Fi 2.4GHz) can be used at a bandwidth of 22MHZ and others. Changing the bandwidth of the system gives the number of channels that can run without overlap, for example, channels 1, 6, and 11 do not overlap. Similarly, we know from [18] that for 5GHz Wi-Fi aka 802.11 ac we use a 160MHz bandwidth, since the frequency bands do not generally have an overlap.

Further examples like T-Mobile's [19] in the cellular connections show that for 4G and 5G cellular connection we use a 15MHz and 100MHz bandwidths.

In the system that has been developed as part of this thesis, multiple scenarios have been taken in to account. Details about this are presented in the next chapter.

2.2.3 Fading Losses and Range Calculation

When considering a communication network utilizing radio waves, there are losses that are incurred by the waves as they travel through a medium. Two types of losses are commonly accounted for in radio waves, as mentioned in the beginning of this chapter.

2.2.3.1 Large Scale Losses

While using radio to communicate across a distance, range capability is inevitably a primary concern. To determine the quality robustness, and range of any RF communication link primarily depends on the physical behavior of the electromagnetic waves.

Harald T. Friis, a Danish-American radio engineer in 1946, presented the Friis Transmission formula. It is defined as "The Friis transmission formula is used in telecommunications engineering, equating the power at the terminals of a receive antenna as the product of power density of the incident wave and the effective aperture of the receiving antenna under idealized conditions given another antenna some distance away transmitting a known amount of power." [20].

In his original idea Friis' formula was to dispense with the use of directivity or gain when describing antenna performance. The figure below explains in brief the way that Friis had explained his equation for an Isotropic transmitting antenna and a receiver on which the EM waves would "fall" in an effective area.

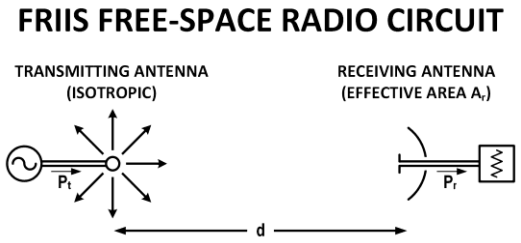

Figure 4 Friis Free Space Radio Circuit [21]

In his original idea Friis' formula was to dispense with the use of directivity or gain when describing antenna performance. The formula presented in [21] was:

$$\frac{P_r}{P_t} = \left(\frac{A_r A_t}{d^2 \lambda^2}\right) \quad (2.3)$$

Where,

- P_t is the power fed into the transmitting antenna input terminals.
- P_r is the power available at receiving antenna output terminals.
- A_r is the effective aperture area of the receiving antenna.
- A_t is the effective aperture area of the transmitting antenna.
- d is the distance between antennas.
- λ is the wavelength of the radio frequency.
- P_t and P_r are in the same units of power.
- A_r, A_t ,d^2 , and λ are in the same units.
- Distance d large enough to ensure a plane wave front at the receive antenna sufficiently approximated by $d = 2a^2/\lambda$ where a is the largest linear dimension of either of the antennas.

In the contemporary format of the formula, it is presented as:[22]

$$P_r = P_t G_t G_r \left(\frac{\lambda}{4\pi}\right)^2 \left(\frac{1}{d}\right)^n \quad (2.4)$$

Where:

- P_r is the power at the receiver. (watts).
- P_t is the power that is generated at the transmitter (watts).
- G_t is the gain of the transmission antenna (scalar).
- G_r is the gain of the receiving antenna (scalar).
- λ is the wavelength (metric or English)
- d is the distance separating transmitter and receiver.
- n is the exponent for environmental conditions (n=2 defines 'free space').

Calculation for communication power in free space propagation of the wave becomes easier when done in the logarithmic scale, i.e., decibels or dB. The Friis equation in this format takes the following shape:

$$P_r[dBm] = P_t[dBm] - L[dBm] - p_\zeta[dB] \quad (2.5)$$

Where:

- P_t is the transmitted power from the ABS.
- P_r is the received power at the receiver antenna, first at R-UAV.
- L is the large scale fading to be calculated using log model of the Friis Equation
- p_ζ is the small-scale fading received from the Rice probability density function (PDF) and calculated using the parameters of the Rician Factor K.

The mentioned log model of the Friis equation is given as:

$$P_r(dB) = -20\log\left(\frac{4\pi}{\lambda}\right) - 10n\log(d) + G_t + G_r + P_t \quad (2.6)$$

The values of power loss due to the gain of the transmitting and receiving antenna and the power at the transmitter all shown in equation (2.6) are presented in dB.

Different values of n are present in different environments.

Table 1 Values for "n"[22]

Environment	"n" value
Free Space	2
Grocery Store	1.8
Retail Store	2.2
Office (hard walls)	3
Office (soft walls)	2.6
Remote keyless entry	4

2.2.3.2 Small Scale Losses

When considering the losses incurred by radio waves during propagation within an area there are two kinds of losses, as mentioned earlier. Figure 5 shows two kinds of losses. This subsection discusses the small-scale losses, also known as non-line of sight (NLOS) losses.

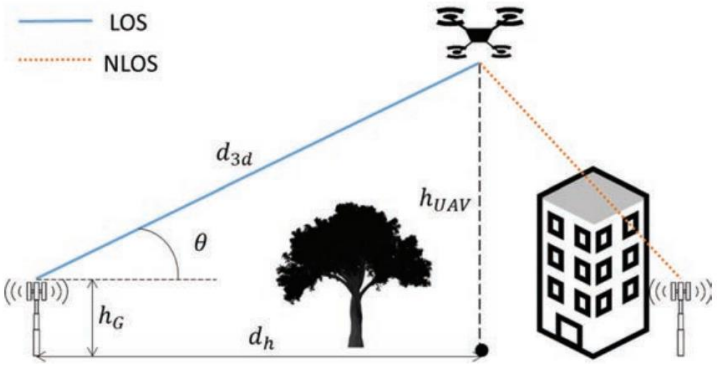

Figure 5 Air to Ground propagation [14]

The small-scale losses in a multipath radio wave propagation can be determined using Rician Fading model. The channel characterization for this is done using the Rice Probability Density Function which is given as:

$$f(x|v,\sigma) = \frac{x}{\sigma^2}\exp\left(\frac{-(x^2+v^2)}{2\sigma^2}\right) I_o\left(\frac{xv}{\sigma^2}\right) \quad (2.7)$$

The terms in the above function are based on the Rician PDF (probability density function) as mentioned earlier, these are based on the distribution of random variables in the cartesian space which have a non-zero mean. The function $f(x|v,\sigma)$ can be used to determine the probability of a point lying on the within the Rician distribution where the value of v and σ are the distance of the point in the cartesian space and the standard deviation of the number distribution in the cartesian space. The value of I_o is the modified Bessel function of the first kind with order zero.

The average power that is received at the Rx can be calculated as:

$$P_r = \int z^2 p_z(z) dz = s^2 + 2\sigma^2 \quad (2.8)$$

The power per unit of area $(z^2)$of the signal at a distance z can be written as $p_z(z)$. The determination of the average power in a specified area due to the power density from a transmitter, after small scale fading losses can be determined as is shown in equation (2.8). This value is presented in dB.

The inclusion of the small scale fading in UAV communication has not been considered when setting up the simulation of the system, but values can be input into the system. In [23] certain methods for the estimation of the Rician Factor K have been presented.

The next chapter will discuss some of the ways that the above parameters can be used in the calculation of range for communication and tie that in with the collision/rendezvous cone theory for the guidance laws.

Chapter 3 Application of UAVs in Wireless Communication

In this chapter, ways to implement the parameters used in the definition of the wireless networks and rendezvous cones for determination of a guidance law are presented. The chapter is further divided, first to get a closer look at how collision cones are defined and how the same theory can be used in the implementation of the rendezvous cone and to determine the range of a wireless network based on the parameters from chapter 2. The final subsection is used for describing the derivation of the guidance law for UAVs in the wireless network for 2, 3 and multiple UAVs.

3.1 Collision and Rendezvous Cones

Many of the data that is known for guidance using conventional methods involves the use of proportional navigation (PN) and similar techniques. These techniques present a good way to implement a guidance law for collision and collision avoidance for point objects. However, the proportional navigation method and its iterations do not consider the shape of the objects and the effects of these shapes on the collision avoidance techniques.

Collision cones are an approach for guidance and ideally suited for automated guided vehicles or autonomous robots. The roots of the techniques lie within the realm of aerospace engineering unlike most other techniques in the robotics world as presented in references used by [4]. In [4], the authors develop the collision cone theory to describe the conditions for collision and techniques to account for the shape of the objects involved. Using similar techniques in [25], researchers have created safe passage cones and rendezvous cones for guidance of objects

moving in space. We have used the same techniques in the development of the guidance laws in our scenario.

3.1.1 Collision conditions between objects

To understand the conditions for collision between a point and circular object let's look at an example from [4]. In Figure 6 below, the geometry for the collision cone between a point and a circle.

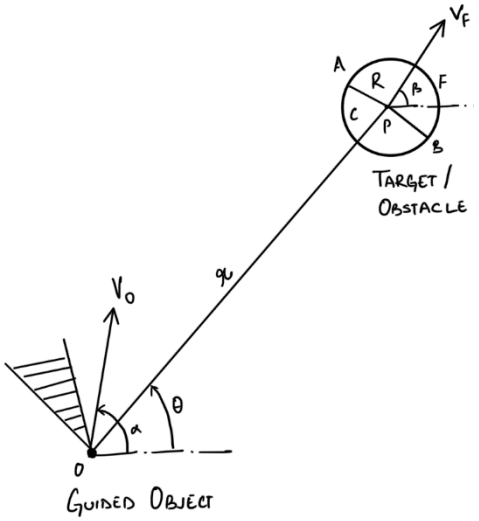

Figure 6 Collision Geometry between a point and circle

The collision cone can be used to check for conditions that would lead to collision between the objects. The collision cone is defined as the set such as if the velocity vector of the point object lies inside this set, this causes a collision. In Figure 6 the object F is a circle of radius R and velocity v_F and the point object is O with a velocity vector v_O. The hatched triangle is a 2-dimensional representation of the collision cone. The velocity vector, if within the boundaries of the collision cone will lead to a condition that is necessary and sufficient for the collision between the object and the target/obstacle shall occur

We determine the following states for the interaction between the point and circular object:

- r is the distance between the center of the circle and the object.
- θ is the angle made by the line joining the center of the circle and the point object with respect to a reference.
- $V_r = \dot{r}$ is the rate of change of the distance r between the point and circular object.
- $V_\theta = r\dot{\theta}$ is the rate of change of angle due to the movement of the objects.

The conditions for the collision between the objects are given in [4]:

$$Condition\ 1 \qquad r^2V_\theta^2 < R^2\left(V_r^2 + V_\theta^2\right) \qquad (3.1)$$

$$Condition\ 2 \qquad V_r < 0 \qquad (3.2)$$

If conditions in equation 3.1 and 3.2 are met, collision between the two objects is imminent. Using the above system of equations, a guidance law that would drive an object on a collision course towards another object can be found. In [24], the authors have presented a method using the techniques mentioned above for guidance related with a rendezvous cone.

The R value in equation 3.1 is the measure of the sum of the radii of the two objects. Equation 3.1 can be converted into the following parameter.

$$y = r^2V_\theta^2 - R^2(V_r^2 + V_\theta^2) \qquad (3.3)$$

Thus, using information on the parameter y the equations 3.1 and 3.2 can be changed to:

$$Condition\ 1 \qquad y < 0 \qquad (3.4)$$

$$Condition\ 2 \qquad V_r < 0 \qquad (3.5)$$

For a value of $y = 0$ it is observed that the two objects (considered circle) graze each other.

Further a parameter "$e = \ R - w$" can be used instead of R and the y parameter is then defined as:

$$y = r^2 V_\theta^2 - e^2 (V_r^2 + V_\theta^2) \qquad (3.6)$$

The addition of this e parameter into the equation can thus be used for manipulating the overlap or gap between the two circles, for example, setting the value of w = 0 and driving the value of y to 0 would lead to a grazing condition between the two objects.

To drive the value of the parameter y to zero, dynamic inversion method has been used. Calculation of the acceleration value to be applied on the guided object would thus be based on the feedback of values of the state space variables of the engagement.

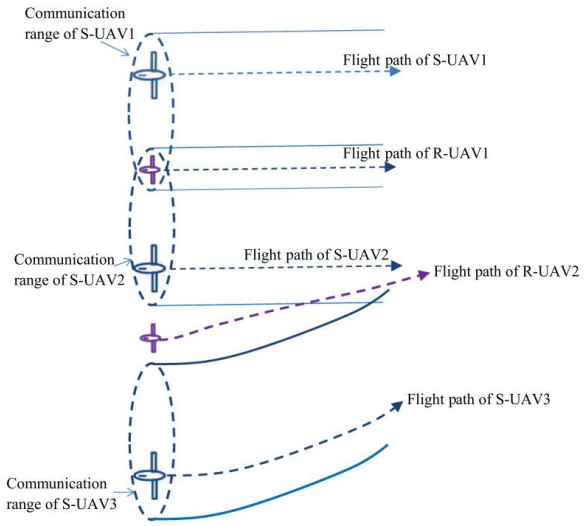

Figure 7 Maintenance of Communication in mobile networks [24]

The image above labelled Figure 7 [24] shows how the rendezvous cone can be used to guide the movement of UAVs for maintaining communication network. The system is developed based on the above example.

Consider three UAVs:

a. **ABS (aerial base station)**: consider that the A2G communication is instantaneous and there is no latency for the ease of modeling.

b. **Relay UAV (R-UAV):** Uses the collision cone guidance law for navigation between the ABS and AUE.

c. **AUE (Aerial User Equipment):** Final recipient of the propagation wave in the 3 UAV system where the SNR is measured against the threshold SNR for the system.

For various wavelengths, and bandwidth values for different networks, using concepts detailed above in Chapter 2, the losses and thus communication radii network can thus be calculated using the following steps:

$$wavelenghtloss\ (loss\ at\ 1m) = 20 * \log\left(\frac{\lambda}{4\pi}\right) \tag{3.7}$$

Where λ is the wavelength of the propagation/ communication system wave.

Now based on the Friis equation define a term as:

$$a_{TxRx} = \frac{noisefloor - PtdB + Tx_{gain} + Rx_{gain} + SNR_T - wavelengthloss}{10\eta} \tag{3.8}$$

Where:

- noisefloor can be calculated as shown in equation (2.1) & can be converted to dB by log(kTB).
- $PtdB$ is the power of the transmitter in dB
- Tx_{gain} is the antenna gain of the transmitter.
- Rx_{gain} is the antenna gain of the receiver.
- SNR_T is the threshold SNR value of the system.

Communication range *"d"* can be obtained as:

$$d = 10^{-a_{TxRx}} \tag{3.9}$$

Based on equation 3.35 the communication range for various systems are as follows:

1. Wi-Fi
   a. **Wi-Fi 2.4:**

      For a wave Frequency 2.4 GHz and the bandwidths as follows:

      i. Bandwidth (BW) of 20 MHz has a communication range of 219.050 m
      ii. BW of 40 MHz has a communication range of 154.8917 m
      iii. BW of 80 MHz has a communication range of 109.5250 m
      iv. BW of 160 MHz has a communication range of 77.4459 m

   b. **Wi-Fi 5:**

      For a wave Frequency 5 GHz and the bandwidths as follows:

      i. BW of 20 MHz has a communication range of 105.144 m
      ii. BW of 40 MHz has a communication range of 74.3480 m
      iii. BW of 80 MHz has a communication range of 52.5720 m
      iv. BW of 160 MHz has a communication range of 37.1740 m

2. Cellular
   a. LTE: Wave Frequency 700 MHz
      i. BW of 1.4 MHz has a communication range of 2838.6 m
      ii. BW of 3 MHz has a communication range of 1939.1 m
      iii. BW of 5 MHz has a communication range of 1502.1m
      iv. BW of 10 MHz has a communication range of 1062.1 m

v. BW of 15 MHz has a communication range of 867.2130 m

b. 5G cellular: Wave Frequency 28GHz

i. BW of 100 MHz has a communication range of 8.3968 m

ii. BW of 200 MHz has a communication range of 5.9374 m

iii. BW of 300 MHz has a communication range of 4.8479 m

iv. BW of 400 MHz has a communication range of 4.1984 m

3.1.2 Guidance laws for application in communication network

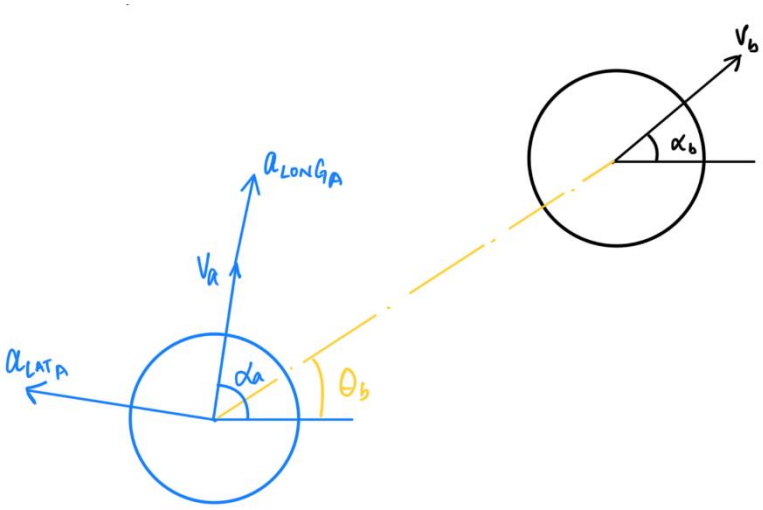

Figure 8 Multi-Object Interaction

Refer Figure 8, which two UAVs. With their communication radii modeled by circles. Define two quantities y_{1_b} and y_{2_b} as follows:

$$y_{1b} = r_b^2 V_{\theta b}^2 - e_b^2\left(V_{rb}^2 + V_{\theta b}^2\right) \tag{3.10}$$

$$y_{2b} = \left(V_{rb}^2 + V_{\theta b}^2\right) \tag{3.11}$$

In these equations y_{1_b} represents the collision cone function defined earlier and y_{2_b} represents the relative velocity between the two UAVs. By driving y_{1_b} and y_{2_b} to zero, the two UAVs will be on a trajectory whereby, they can achieve a communication link.

To facilitate, matching the course of trajectory between the two UAVs would enable a longer interaction and thus a stronger network connection for a longer duration. The quantities $V_{rb}\ and\ V_{\theta b}$ are shown in the equations below, this are defined as the rate of change of distance and angle of the line of sight between the two UAVs respectively.

$$V_{rb} = v_b \cos(\alpha_b - \theta_b) - v_a \cos(\alpha_a - \theta_b) \quad (3.12)$$

$$V_{\theta b} = v_b \sin(\alpha_b - \theta_b) - v_a \sin(\alpha_a - \theta_b) \quad (3.13)$$

$$\theta_b = \tan^{-1}\left(\frac{y_b - y_a}{x_b - x_a}\right) \quad (3.14)$$

The state space equations between the base station UAV and the relay UAV are:

$$\dot{r_b} = V_{rb} \quad (3.15)$$

$$\dot{\theta_b} = \frac{V_{\theta b}}{r_b} \quad (3.16)$$

$$\dot{V}_{rb} = \frac{V_{\theta b}^2}{r_b} + a_{lat_a} \sin(\alpha_a - \theta_b) - a_{long_a} \cos(\alpha_a - \theta_b) \quad (3.17)$$

$$\dot{V}_{\theta b} = \frac{-V_{rb} V_{\theta b}}{r_b} - a_{lat_a} \cos(\alpha_a - \theta_b) - a_{long_a} \sin(\alpha_a - \theta_b) \quad (3.18)$$

To determine the acceleration values a_{lat} and a_{long}, a dynamic inversion y_{1b} and y_{2b} must be performed. We obtain the following derivative terms

$$\frac{\partial y_{1b}}{\partial r_b} \dot{r_b} = 2 r_b V_{\theta b}^2 V_{rb} \quad (3.19)$$

$$\frac{\partial y_{1b}}{\partial V_{rb}} \dot{V}_{rb} = -2 e_b^2 V_{rb} \dot{V}_{rb} \quad (3.20)$$

$$\frac{\partial y_{1b}}{\partial V_{\theta b}} \dot{V}_{\theta b} = 2(r_b^2 - e_b^2) V_{\theta b} \dot{V}_{\theta b} \quad (3.21)$$

For the above from dynamic inversion, the following equations come up:

$$\dot{y}_{1b} = -K_{1b} y_{1b} \quad (3.22)$$

$$\dot{y}_{1b} = \frac{\partial y_{1b}}{\partial r_b} \dot{r_b} + \frac{\partial y_{1b}}{\partial V_{rb}} \dot{V}_{rb} + \frac{\partial y_{1b}}{\partial V_{\theta b}} \dot{V}_{\theta b} \quad (3.23)$$

Thus, from substitution of the partial derivatives in the above equation, we get:

$$-K_{1b} y_{1b} = a_{lat_a}(-2V_{rb} e_b^2 \sin(\alpha_a - \theta_b) - 2(r_b^2 - e_b^2) V_{\theta b} \cos(\alpha_a - \theta_b)) \quad (3.24)$$
$$- a_{long_a}(-2V_{rb} e_b^2 \cos(\alpha_a - \theta_b)$$
$$+ 2(r_b^2 - e_b^2) V_{\theta b} \sin(\alpha_a - \theta_b))$$

Simplifying the system and defining u_{1_b} and u_{2_b} as follows and substitution of those values in equation (3.21) gives:

$$-K_{1b} y_{1b} = a_{lat_a}(A_b \sin(\alpha_a - \theta_b) + B_b \cos(\alpha_a - \theta_b)) \quad (3.25)$$
$$- a_{long_a}(A_b \cos(\alpha_a - \theta_b) + B_b \sin(\alpha_a - \theta_b))$$

$$u_{1b} = A_b \sin(\alpha_a - \theta_b) - B_b \cos(\alpha_a - \theta_b)$$

$$u_{2b} = A_b \cos(\alpha_a - \theta_b) + B_b \sin(\alpha_a - \theta_b) \quad (3.26)$$

$$-K_{1b} y_{1b} = a_{lat_a} u_{1b} - a_{long_a} u_{2b} \quad (3.27)$$

$$\frac{\partial y_{2b}}{\partial V_{rb}} \dot{V_{rb}} = 2V_{rb} \dot{V_{rb}} \quad (3.28)$$

$$\frac{\partial y_{2b}}{\partial V_{\theta b}} \dot{V_{\theta b}} = 2V_{\theta b} \dot{V_{\theta b}} \quad (3.29)$$

Like the above dynamic inversion:

$$\therefore -K_{2b} y_{2b} = a_{lat_a}(2V_{rb} \sin(\alpha_a - \theta_b) - 2V_{\theta b} \cos(\alpha_a - \theta_b)) \quad (3.30)$$
$$- a_{long_a}(2V_{rb} \cos(\alpha_a - \theta_b) + 2V_{\theta b} \sin(\alpha_a - \theta_b))$$

The terms can be defined as:

$$u_{3b} = (2V_{rb}\sin(\alpha_a - \theta_b) - 2V_{\theta b}\cos(\alpha_a - \theta_b)) \quad (3.31)$$

$$u_{4b} = (2V_{rb}\cos(\alpha_a - \theta_b) + 2V_{\theta b}\sin(\alpha_a - \theta_b)) \quad (3.32)$$

Then using (3.31) and (3.32), equation (3.30) can be written as:

$$\therefore -K_{2b}y_{2b} = a_{lat_a}u_{3b} - a_{long_a}u_{4b} \quad (3.33)$$

Using equations (3.25) and (3.33) the following is determined:

$$a_{long_a} = \frac{-K_{1b}y_{1b}u_{3b} + K_{2b}y_{2b}u_{1b}}{u_{4b}u_{1b} - u_{2b}u_{3b}} \quad (3.34)$$

$$a_{lat_a} = \frac{-K_{1b}y_{1b}u_{4b} + K_{2b}y_{2b}u_{2b}}{u_{4b}u_{1b} - u_{2b}u_{3b}} \quad (3.35)$$

The guidance law based on (3.34) and (3.35) can be used for rendezvous and course matching between two objects. Using the same concept, redefining the distance R and "$e = R - w$" as the radius of communication, the guidance law creates a motion trajectory for the guided object to facilitate by the communication between the UAVs.

For proper determination of the guidance law for the system as mentioned in the statement above, defining some steps and certain object names would make the subsequent derivation of the guidance law more organized and thus easier for interpretation.

Using the interaction as presented between the two objects in section 3.1.2 and further using the acceleration values from equations (3.34) and (3.35) the calculation can be further done as:

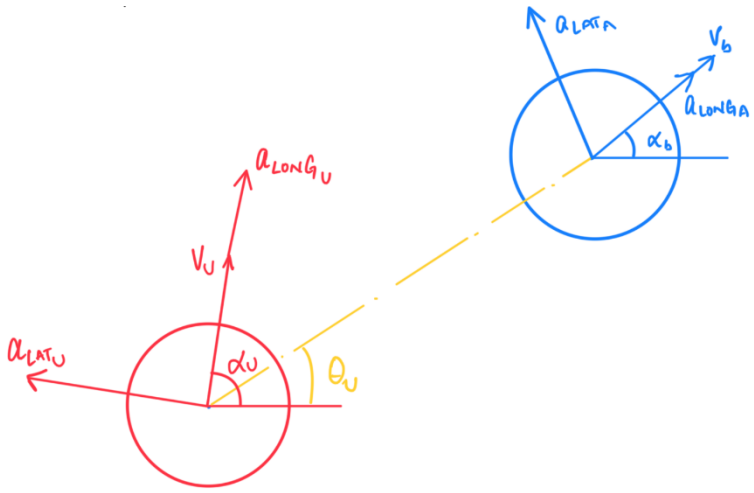

Figure 9 Interaction between R-UAV and AUE

For the interaction shown in Figure 9 guidance laws are derived for the follower UAV (shown in red) with the consideration of acceleration present on the leader UAV (shown in blue). The derivation of the guidance laws is presented below:

$$V_{ru} = v_a \cos(\alpha_a - \theta_u) - v_a \cos(\alpha_u - \theta_u) \tag{3.36}$$

$$V_{\theta u} = v_a \sin(\alpha_a - \theta_u) - v_u \sin(\alpha_u - \theta_u) \tag{3.37}$$

$$\theta_u = \tan^{-1}\left(\frac{y_a - y_u}{x_a - x_u}\right) \tag{3.38}$$

The state space equations for the interaction are:

$$\dot{r_u} = V_{ru} \tag{3.39}$$

$$\dot{\theta_u} = \frac{V_{\theta u}}{r_u} \tag{3.40}$$

$$\dot{V}_{ru} = \frac{V_{\theta u}^2}{r_u} + a_{lat_u} \sin(\alpha_u - \theta_u) - a_{lat_a} \sin(\alpha_a - \theta_u) + a_{long_a} \cos(\alpha_a - \theta_u) - a_{long_u} \cos(\alpha_u - \theta_u) \tag{3.41}$$

$$\dot{V}_{\theta u} = \frac{-V_{ru}V_{\theta u}}{r_b} + a_{lat_a}\cos(\alpha_a - \theta_u) + a_{long_a}\sin(\alpha_a - \theta_u) \tag{3.42}$$

$$- a_{lat_u}\cos(\alpha_u - \theta_u) - a_{long_u}\sin(\alpha_u - \theta_u)$$

$$y_{1u} = r_u^2 V_{\theta u}^2 - e_u^2\left(V_{ru}^2 + V_{\theta u}^2\right) \tag{3.43}$$

$$y_{2u} = \left(V_{ru}^2 + V_{\theta u}^2\right) \tag{3.44}$$

Like earlier calculation the acceleration using the dynamic inversion would be as follows:

$$\frac{\partial y_{1u}}{\partial r_u}\dot{r_u} = 2r_u V_{\theta u}^2 V_{ru} \tag{3.45}$$

$$\frac{\partial y_{1u}}{\partial V_{ru}}\dot{V_{ru}} = -2e_u^2 V_{ru}\dot{V_{ru}} \tag{3.46}$$

$$\frac{\partial y_{1u}}{\partial V_{\theta u}}\dot{V}_{\theta u} = 2(r_u^2 - e_u^2)V_{\theta u}\dot{V}_{\theta u} \tag{3.47}$$

Similarly, the calculation leads to the equation as shown below:

$$\therefore\ -K_{1u}y_{1u} = a_{lat_u}u_{1uu} - a_{long_u}u_{2uu} + a_{long_a}u_{2ua} - a_{lat_a}u_{1ua} \tag{3.48}$$

Where:

$$u_{1uu} = A_u\sin(\alpha_u - \theta_u) - B_u\cos(\alpha_u - \theta_u) \tag{3.49}$$

$$u_{2uu} = A_u\cos(\alpha_u - \theta_u) + B_u\sin(\alpha_u - \theta_u) \tag{3.50}$$

$$u_{1ua} = A_u\sin(\alpha_a - \theta_u) - B_u\cos(\alpha_a - \theta_u) \tag{3.51}$$

$$u_{2ua} = A_u\cos(\alpha_a - \theta_u) + B_u\sin(\alpha_a - \theta_u) \tag{3.52}$$

$$A_u = -2e_u^2 V_{ru}\ ; B_u = 2(r_u^2 - e_u^2)V_{\theta u} \tag{3.53}$$

Further,

$$c_{1u} = -K_{1u}y_{1u} - a_{long_a}u_{2ua} + a_{lat_a}u_{1ua} \tag{3.54}$$

$$c_{2u} = -K_{2u}y_{2u} - a_{long_a}u_{4ua} + a_{lat_a}u_{3a} \tag{3.55}$$

Where:

$$u_{3uu} = 2V_{ru}\sin(\alpha_u - \theta_u) - 2V_{\theta u}\cos(\alpha_u - \theta_u) \tag{3.56}$$

$$u_{4uu} = 2V_{ru}\cos(\alpha_u - \theta_u) + 2V_{\theta u}\sin(\alpha_u - \theta_u) \tag{3.57}$$

$$u_{3ua} = 2V_{ru}\sin(\alpha_a - \theta_u) - 2V_{\theta u}\cos(\alpha_a - \theta_u) \tag{3.58}$$

$$u_{4ua} = 2V_{ru}\cos(\alpha_a - \theta_u) + 2V_{\theta u}\sin(\alpha_a - \theta_u) \tag{3.59}$$

Solving the above mentioned the acceleration is calculated as:

$$a_{long_u} = \frac{c_{1u}u_{4uu} - c_{2u}u_{2uu}}{u_{4uu}u_{1uu} - u_{2uu}u_{3uu}} \tag{3.60}$$

$$a_{lat_u} = \frac{c_{1u}u_{3uu} - c_{2u}u_{1uu}}{u_{4uu}u_{1uu} - u_{2uu}u_{3uu}} \tag{3.61}$$

The above calculation is the basis for an interaction between another user that could work as a follower to the first user. Simulations for movement in different networks are presented in Chapter 4. The calculation for the system is shown below, the section 3.2.1 shows the calculation.

3.1.3 Guidance laws for follower AUE based on first AUE's trajectory.

In this section the guidance laws for the movement of a follower AUE UAV are based on the trajectory of the UAV that precedes it. The movement of each of the UAV that further follows will be based on the movement of the UAV that is subsequently following another AUE, up until the R-UAV, which further is following the ABS.

For the interaction:

$$V_{r_{12}} = v_1 \cos(\alpha_1 - \theta_{12}) - v_2 \cos(\alpha_2 - \theta_{12}) \tag{3.62}$$

$$V_{\theta_{12}} = v_1 \sin(\alpha_1 - \theta_{12}) - v_2 \sin(\alpha_2 - \theta_{12}) \tag{3.63}$$

$$\theta_{12} = \tan^{-1}\left(\frac{y_1 - y_2}{x_1 - x_2}\right) \tag{3.64}$$

The state space equations for the interaction:

$$\dot{r_{12}} = V_{r_{12}} \tag{3.65}$$

$$\dot{\theta_{12}} = \frac{V_{\theta_{12}}}{r_{12}} \tag{3.66}$$

$$\dot{V}_{r_{12}} = \frac{V_{\theta_{12}}^2}{r_{12}} + a_{lat_2} \sin(\alpha_2 - \theta_{12}) - a_{lat_1} \sin(\alpha_1 - \theta_{12}) + a_{long_1} \cos(\alpha_1 - \theta_{12}) - a_{long_2} \cos(\alpha_2 - \theta_{12}) \tag{3.67}$$

$$\dot{V}_{\theta_{12}} = \frac{-V_{r_{12}} V_{\theta_{12}}}{r_{12}} + a_{lat_1} \cos(\alpha_1 - \theta_{12}) + a_{long_1} \sin(\alpha_1 - \theta_{12}) - a_{lat_2} \cos(\alpha_2 - \theta_{12}) - a_{long_2} \sin(\alpha_2 - \theta_{12}) \tag{3.68}$$

$$y_{1_{12}} = r_{12}^2 V_{\theta_{12}}^2 - e_{12}^2 \left(V_{r_{12}}^2 + V_{\theta_{12}}^2\right) \tag{3.69}$$

$$y_{2_{12}} = \left(V_{r_{12}}^2 + V_{\theta_{12}}^2\right) \tag{3.70}$$

Like earlier calculate the acceleration using the dynamic inversion:

$$\frac{\partial y_{1_{12}}}{\partial r_{12}}\dot{r}_{12} = 2r_{12}V_{\theta_{12}}^2 V_{r_{12}} \tag{3.71}$$

$$\frac{\partial y_{1_{12}}}{\partial V_{r_{12}}}\dot{V}_{r_{12}} = -2e_{12}^2 V_{r_{12}}\dot{V}_{r_{12}} \tag{3.72}$$

$$\frac{\partial y_{1_{12}}}{\partial V_{\theta_{12}}}\dot{V}_{\theta_{12}} = 2(r_{12}^2 - e_{12}^2)V_{\theta_{12}}\dot{V}_{\theta_{12}} \tag{3.73}$$

In the similar way the calculation leads to the equation as shown below:

$$\therefore\ -K_{1_{12}}y_{1_{12}} = a_{lat_2}u_{1_{22}} - a_{long_2}u_{2_{22}} + a_{long_1}u_{2_{21}} - a_{lat_1}u_{1_{21}} \tag{3.74}$$

Where:

$$u_{1_{22}} = A_{21}\sin(\alpha_2 - \theta_{12}) - B_{21}\cos(\alpha_2 - \theta_{12}) \tag{3.75}$$

$$u_{2_{22}} = A_{21}\cos(\alpha_2 - \theta_{12}) + B_{21}\sin(\alpha_2 - \ \theta_{12}) \tag{3.76}$$

$$u_{1_{21}} = A_{21}\sin(\alpha_1 - \theta_{12}) - B_{21}\cos(\alpha_1 - \theta_{12}) \tag{3.77}$$

$$u_{2_{21}} = A_{21}\cos(\alpha_1 - \theta_{12}) + B_{21}\sin(\alpha_1 - \ \theta_{12}) \tag{3.78}$$

$$A_{21} = \ -2e_{12}^2 V_{r_{12}}\ ; B_{21} = 2(r_{12}^2 - e_{12}^2)V_{\theta_{12}} \tag{3.79}$$

Further,

$$c_{1_{21}} = \ -K_{1_2}y_{1_{12}} - a_{long_1}u_{2_{21}} + a_{lat_1}u_{1_{21}} \tag{3.80}$$

$$c_{2_{21}} = \ -K_{2_2}y_{2_{12}} - a_{long_1}u_{4_{21}} + a_{lat_1}u_{3_{21}} \tag{3.81}$$

Where:

$$u_{3_{22}} = 2V_{r_{12}}\sin(\alpha_2 - \theta_{12}) - 2V_{\theta_{12}}\cos(\alpha_2 - \theta_{12}) \tag{3.82}$$

$$u_{4_{22}} = 2V_{r_{12}}\cos(\alpha_2 - \theta_{12}) + 2V_{\theta_{12}}\sin(\alpha_2 - \ \theta_{12}) \tag{3.83}$$

$$u_{3_{21}} = 2V_{r_{12}}\sin(\alpha_1 - \theta_{12}) - 2V_{\theta_{12}}\cos(\alpha_1 - \theta_{12}) \tag{3.84}$$

$$u_{4_{21}} = 2V_{r_{12}}\cos(\alpha_1 - \theta_{12}) + 2V_{\theta_{12}}\sin(\alpha_1 - \ \theta_{12}) \tag{3.85}$$

Solving the above equation for the acceleration values:

$$a_{long_2} = \frac{c_{1_{21}} u_{4_{22}} - c_{2_{21}} u_{2_{22}}}{u_{4_{22}} u_{1_{22}} - u_{2_{22}} u_{3_{22}}} \tag{3.86}$$

$$a_{lat_2} = \frac{c_{1_{21}} u_{3_{22}} - c_{2_{21}} u_{1_{22}}}{u_{4_{22}} u_{1_{22}} - u_{2_{22}} u_{3_{22}}} \tag{3.87}$$

3.2 Generalized guidance laws for follower UAVs in an n-UAV Systems

Based on the calculations that has been presented in the previous section, the calculation for the nth UAV in an n-UAV system is presented in this section. The acceleration that is derived from the guidance law shows that the movement of the n^{th} UAV is based on the $(n-1)^{th}$ UAV in the system.

Like the calculation we have done for the interaction between the first and the second user, we can generalize the solution to:

For the interaction we have

$$a_{long_2} V_{r_{(n-1)(n)}} = v_{(n-1)} \cos\left(\alpha_{(n-1)} - \theta_{(n-1)(n)}\right) - v_{(n)} \cos\left(\alpha_{(n)} - \theta_{(n-1)(n)}\right) \tag{3.88}$$

$$V_{\theta_{(n-1)(n)}} = v_{(n-1)} \sin\left(\alpha_{(n-1)} - \theta_{(n-1)(n)}\right) - v_{(n)} \sin\left(\alpha_{(n)} - \theta_{(n-1)(n)}\right) \tag{3.89}$$

$$\theta_{(n-1)(n)} = \tan^{-1}\left(\frac{y_{(n-1)} - y_{(n)}}{x_{(n-1)} - x_{(n)}}\right) \tag{3.90}$$

The state space equations for the interaction we have:

$$\dot{r}_{(n-1)n} = V_{r_{(n-1)(n)}} \tag{3.91}$$

$$\dot{\theta}_{(n-1)(n)} = \frac{V_{\theta_{(n-1)(n)}}}{r_{(n-1)(n)}} \tag{3.92}$$

$$\dot{V}_{r_{(n-1)(n)}} = \frac{V^2_{\theta_{(n-1)(n)}}}{r_{(n-1)(n)}} + a_{lat_{(n-1)}} \sin\left(\alpha_{(n)} - \theta_{(n-1)(n)}\right) - a_{lat_{(n-1)}} \sin\left(\alpha_{(n-1)} - \theta_{(n-1)(n)}\right) + a_{long_{(n-1)}} \cos\left(\alpha_{(n-1)} - \theta_{(n-1)(n)}\right) - a_{long_{(n)}} \cos\left(\alpha_{(n)} - \theta_{(n-1)(n)}\right) \quad (3.93)$$

$$\dot{V}_{\theta_{(n-1)(n)}} = \frac{-V_{r_{(n-1)(n)}} V_{\theta_{(n-1)(n)}}}{r_{(n-1)(n)}} + a_{lat_{(n-1)}} \cos\left(\alpha_{(n-1)} - \theta_{(n-1)(n)}\right) + a_{long_{(n-1)}} \sin\left(\alpha_{(n-1)} - \theta_{(n-1)(n)}\right) - a_{lat_{(n)}} \cos\left(\alpha_{(n)} - \theta_{(n-1)(n)}\right) - a_{long_{(n)}} \sin\left(\alpha_{(n)} - \theta_{(n-1)(n)}\right) \quad (3.94)$$

$$y_{1_{(n-1)(n)}} = r^2_{(n-1)(n)} V^2_{\theta_{(n-1)(n)}} - e^2_{(n-1)(n)} \left(V^2_{r_{(n-1)(n)}} + V^2_{\theta_{(n-1)(n)}}\right) \quad (3.95)$$

$$y_{2_{(n-1)(n)}} = \left(V^2_{r_{(n-1)(n)}} + V^2_{\theta_{(n-1)(n)}}\right) \quad (3.96)$$

Like what we did earlier we would calculate the acceleration using the dynamic inversion:

$$\frac{\partial y_{1_{(n-1)(n)}}}{\partial r_{(n-1)(n)}} \dot{r}_{(n-1)n} = 2 r_{(n-1)(n)} V^2_{\theta_{(n-1)(n)}} V_{r_{(n-1)(n)}} \quad (3.97)$$

$$\frac{\partial y_{1_{(n-1)(n)}}}{\partial V_{r_{(n-1)(n)}}} \dot{V}_{r_{(n-1)n}} = -2 e^2_{(n-1)(n)} V_{r_{(n-1)(n)}} \dot{V}_{r_{(n-1)n}} \quad (3.98)$$

$$\frac{\partial y_{1_{(n-1)(n)}}}{\partial V_{\theta_{(n-1)(n)}}} \dot{V}_{\theta_{(n-1)n}} = 2(r^2_{(n-1)(n)} - e^2_{(n-1)(n)}) V_{\theta_{(n-1)(n)}} \dot{V}_{\theta_{(n-1)n}} \quad (3.99)$$

In the similar way that we did the calculation we would arrive to the equation as shown below:

$$\therefore -K_{1_{(n-1)(n)}} y_{1_{(n-1)(n)}} = a_{lat_{(n)}} u_{1_{(n)(n)}} - a_{long_{(n)}} u_{2_{(n)(n)}} + a_{long_{(n-1)}} u_{2_{(n)(n-1)}} - a_{lat_{(n-1)}} u_{1_{(n)(n-1)}} \quad (3.100)$$

Where:

$$u_{1_{(n)(n)}} = A_{(n)(n-1)} \sin\left(\alpha_{(n)} - \theta_{(n-1)(n)}\right) - B_{(n)(n-1)} \cos\left(\alpha_{(n)} - \theta_{(n-1)(n)}\right) \quad (3.101)$$

$$u_{2_{(n)(n)}} = A_{(n)(n-1)} \cos\left(\alpha_{(n)} - \theta_{(n-1)(n)}\right) + B_{(n)(n-1)} \sin\left(\alpha_{(n)} - \theta_{(n-1)(n)}\right) \quad (3.102)$$

$$u_{1_{(n)(n-1)}} = A_{(n)(n-1)} \sin\left(\alpha_{(n-1)} - \theta_{(n-1)(n)}\right) - B_{(n)(n-1)} \cos\left(\alpha_{(n-1)} - \theta_{(n-1)(n)}\right) \quad (3.103)$$

$$u_{2_{(n)(n-1)}} = A_{(n)(n-1)} \cos\left(\alpha_{(n-1)} - \theta_{(n-1)(n)}\right) + B_{(n)(n-1)} \sin\left(\alpha_{(n-1)} - \theta_{(n-1)(n)}\right) \quad (3.104)$$

$$A_{(n)(n-1)} = -2e^2_{(n-1)(n)} V_{r_{(n-1)(n)}} ; B_{(n)(n-1)} = 2\left(r^2_{(n-1)(n)} - e^2_{(n-1)(n)}\right) V_{\theta_{(n-1)(n)}} \quad (3.105)$$

Further we can define:

$$c_{1_{(n)(n-1)}} = -K_{1_{(n)}} y_{1_{(n-1)(n)}} - a_{long_{(n-1)}} u_{2_{(n)(n-1)}} + a_{lat_{(n-1)}} u_{1_{(n)(n-1)}} \quad (3.106)$$

$$c_{2_{(n)(n-1)}} = -K_{2_{(n)}} y_{2_{(n-1)(n)}} - a_{long_{(n-1)}} u_{4_{(n)(n-1)}} + a_{lat_{(n-1)}} u_{3_{(n)(n-1)}} \quad (3.107)$$

Where:

$$u_{3_{(n)(n)}} = 2V_{r_{(n-1)(n)}} \sin\left(\alpha_{(n)} - \theta_{(n-1)(n)}\right) - 2V_{\theta_{(n-1)(n)}} \cos\left(\alpha_{(n)} - \theta_{(n-1)(n)}\right) \quad (3.108)$$

$$u_{4_{(n)(n)}} = 2V_{r_{(n-1)(n)}} \cos\left(\alpha_{(n)} - \theta_{(n-1)(n)}\right) + 2V_{\theta_{(n-1)(n)}} \sin\left(\alpha_{(n)} - \theta_{(n-1)(n)}\right) \quad (3.109)$$

$$u_{3_{(n)(n-1)}} = 2V_{r_{(n-1)(n)}} \sin\left(\alpha_{(n-1)} - \theta_{(n-1)(n)}\right) - 2V_{\theta_{(n-1)(n)}} \cos\left(\alpha_{(n-1)} - \theta_{(n-1)(n)}\right) \quad (3.110)$$

$$u_{4_{(n)(n-1)}} = 2V_{r_{(n-1)(n)}} \cos\left(\alpha_{(n-1)} - \theta_{(n-1)(n)}\right) + 2V_{\theta_{(n-1)(n)}} \sin\left(\alpha_{(n-1)} - \theta_{(n-1)(n)}\right) \quad (3.111)$$

Solving the above mentioned we get the longitudinal and lateral acceleration for a follower based on the movement trajectory of the leader UAV:

$$a_{long_{(n)}} = \frac{c_{1_{(n)(n-1)}} u_{4_{(n)(n)}} - c_{2_{(n)(n-1)}} u_{2_{(n)(n)}}}{u_{4_{(n)(n)}} u_{1_{(n)(n)}} - u_{2_{(n)(n)}} u_{3_{(n)(n)}}} \quad (3.112)$$

$$a_{lat_{(n)}} = \frac{c_{1_{(n)(n-1)}} u_{3_{(n)(n)}} - c_{2_{(n)(n-1)}} u_{1_{(n)(n)}}}{u_{4_{(n)(n)}} u_{1_{(n)(n)}} - u_{2_{(n)(n)}} u_{3_{(n)(n)}}} \quad (3.113)$$

The equations 3.112 and 3.113 give the longitudinal and lateral acceleration respectively for the n^{th} UAV based on the trajectory that is followed by the $(n-1)^{th}$ UAV.

Chapter 4 Simulation Results for UAVs In Different Network Configurations

In previous chapters, the thesis has shown different network configurations in which the UAVs would move using guidance laws based on collision cone theory. The laws have been presented in Chapter 3. This chapter demonstrates simulation results depicting the performance of the guidance laws.

4.1 Scenario 1: Chain Link Movement in 5G Network

In this scenario the UAVs seek to form a chain link moving in a 5G communication network. The base station is the leader of the pack, the relay UAV seeks to follow the trajectory of the base station, the R-UAV in turn followed by a AUE (aerial user equipment). Below are presented the initial conditions and other factors which can be referenced from the previous chapters.

4.1.1 Initial Conditions and Simulation Parameters

The initial conditions at time t = 0 for the three different UAVs that are moving in this scenario, are shown in Table 2.

Table 2 Scenario 1: Initial Conditions

	Base Station	Relay UAV	End User
Position (x, y) (m)	(-40,20)	(0,0)	(40,20)
Velocity (m/s)	2	5	2
Flight Path Angle (deg)	60°	100°	115°
UAV Physical Radius (m)	2	4	2

Gain values governing the trajectories of the UAVs are given below. These correspond to the rate at which parameters y_1 and y_2 decay in the dynamic inversion laws of equations 3.6, 3.14, and 3.15. Furthermore, these values are presented for the different pairwise interactions

present in this scenario, including the interaction between the base station and the R-UAV and similarly that between the R-UAV and the first AUE. The w value parameter as explained in section 3.1.1 right before equation 3.6 is also. These values are given as:

- **Base Station Communication Circle Penetration** (w_b) : $5m$
- **Relay Station Communication Circle Penetration** (w_r): $5m$
- **Rendezvous Controller Gain (Relay and Base)** (K_{1b}) : 2.5
- **Course Match Controller Gain (Relay and Base)** (K_{2b}): 0.245
- **Rendezvous Controller Gain (Relay and User)** (K_{1u}) : 1.5
- **Course Match Controller Gain (Relay and User)** (K_{2u}) : 0.045

4.1.2 Communication Conditions

As presented in Chapter 2 the conditions for the communication influence the radius of the communication circle. The values associated with the communication system are presented below.

- **Area temperature:** $25\ ^\circ C$
- **Connection Type:** 5G Cellular @ 100 MHz bandwidth
- **Location Type:** Free Space

Table 3 Communication Conditions: Scenario 1

	Base Station	Relay UAV	End User
Power	2W	Variable	–
Tx Gain	20dB	20 dB	–
Rx Gain	–	2 dB	2dB

4.1.3 Simulation Results for Scenario 1

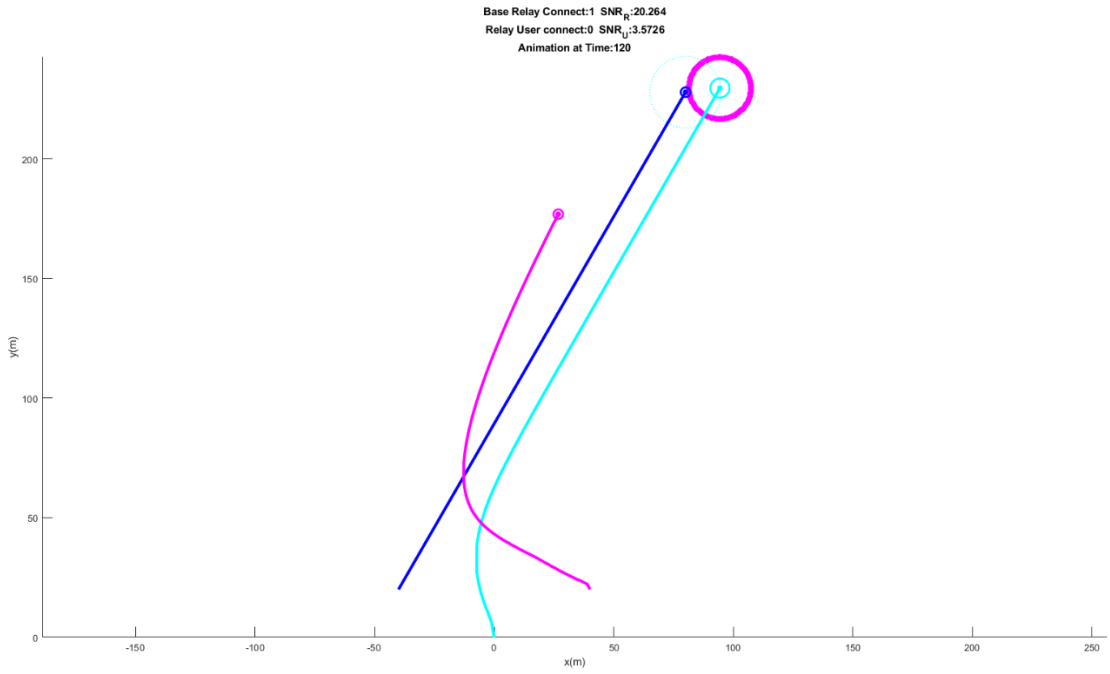

Figure 10 Trajectory plot for Scenario 1

Figure 10 is the last plot related to Scenario 1; the plot is representative of the trajectory that has been followed by the objects in the movement while being using the guidance laws shown earlier in this thesis. Initial conditions for the movement have been presented in Table 2. The object is dark Blue is the aerial base station (ABS), faint cyan circle around is the circle representing the range of communication. The cyan object shows the trajectory of RUAV, the magenta circle around the object is the communication range representation. Finally, the magenta object shows the trajectory of the UE based on the guidance laws, keeping the RUAV as the leader, as the RUAV keeps the ABS as the leader. The text shown above the plot shows the SNR value for the interaction between the RUAV and the ABS (SNR_R) and the RUAV and the AUE(SNR_U). The “Base Relay Connect = 1” and “Relay Use Connect = 0” show the connection status between the two interacting UAVs at the end of the simulation at time t = 120 sec.a

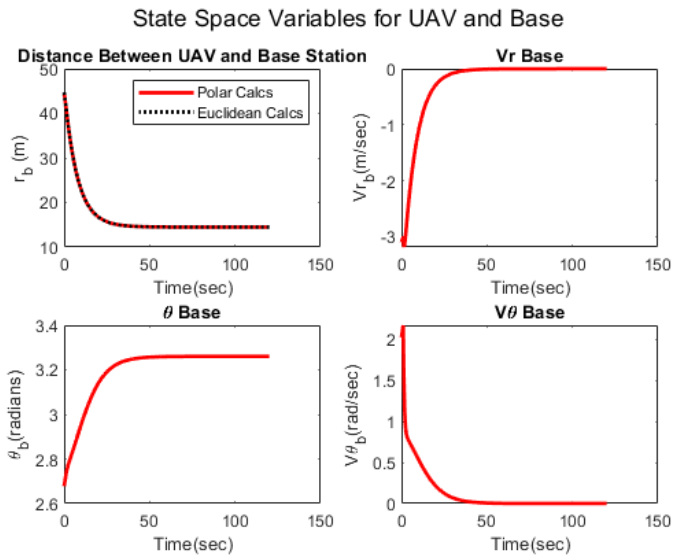

Figure 11 State Space Time History for Interaction between R-UAV and Base Station

Figure 11 shows the time history of the state space variables as the parameter y_1 and y_2 are subjected to dynamic inversion. The top left plot shows the decay of the distance between the Relay UAV and the base station, the red plot shows the value of the state space variable "r", and the dotted black line shows the Euclidean distance calculated at every instant in time. This is done to recognize any errors if they might arise in the calculations through the dynamic inversion. The other plots show the time histories of the state space variable. The top right plot shows the time history of the rate of change of distance between the base station and the R-UAV. The bottom left shows the time history of θ, angle which is made by line joining the R-UAV and base station from a reference, and bottom right shows the time history of V_θ.

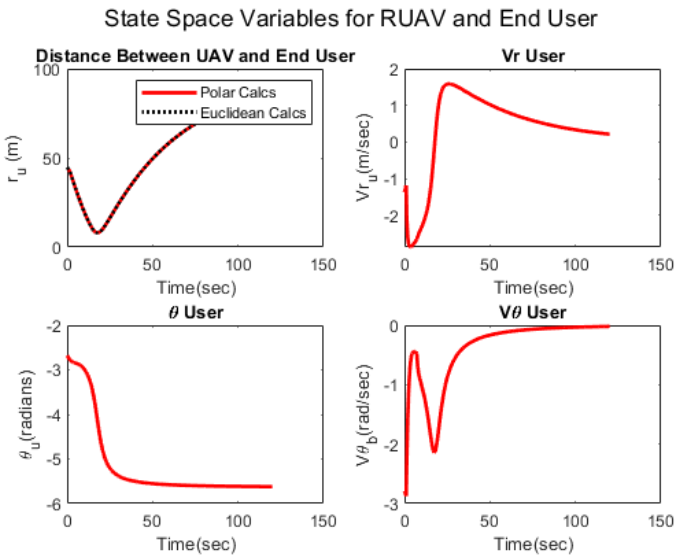

Figure 12 State Space Time History for Interaction between R-UAV and User Equipment

Figure 12 shows a similar interaction between the R-UAV and the UE as was shown in Figure 10 for interaction between R-UAV and the aerial base station.

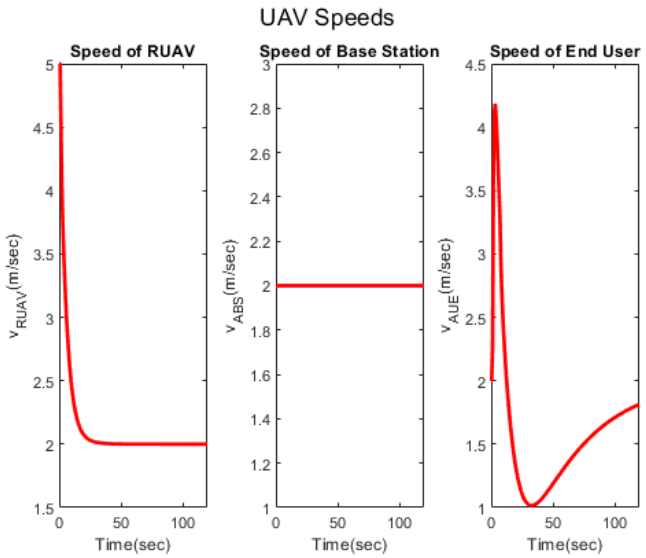

Figure 13 Speed time Histories of the 3 UAVs

Figure 13 shows the time history plots for the speeds of the UAVS, each performing differently based on the acceleration value generated by its guidance law. For example, the left

most plot, shows the time history of the velocity of R-UAV, whose speed reduces from its initial value of $5\ m/s$ to $2\ m/s$ thus matching the speed of the base station. The speed value of the UE also reflects a similar behavior, but since the UE is following the trajectory of the R-UAV, it's speed changes based on the value of the speed of the R-UAV. We also observe here an undershoot value in the speed of the UE, after which the value stabilizes and moves towards aligning with that of the R-UAV. Since the base station is not subject to any acceleration, a constant speed of $2\ m/s$ is observed.

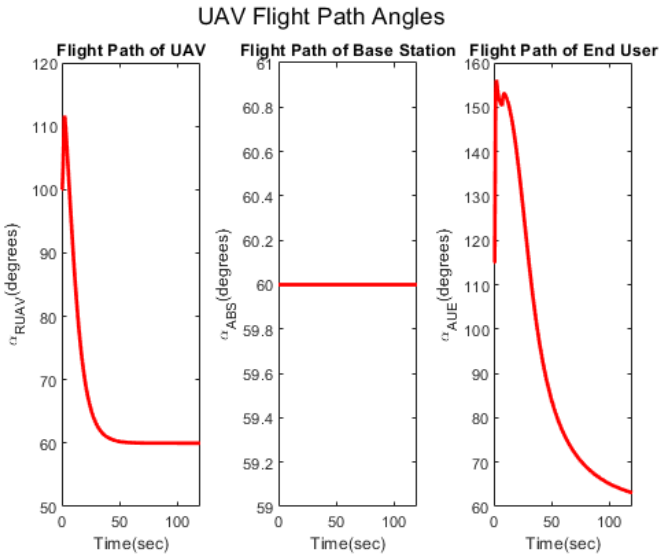

Figure 14 Flight Path Angle Time History

Similar to the plots presented in Figure 13, the plots in Figure 14 show the time history, of flight path angle, in the same order. Going left to right, the value of flight path angle (α) for the R-UAV changes and gets aligned with the base station, (which remains constant, since no acceleration is acting on the base station). The value of the flight path angle of the UE gets aligned with the flight path angle of the R-UAV.

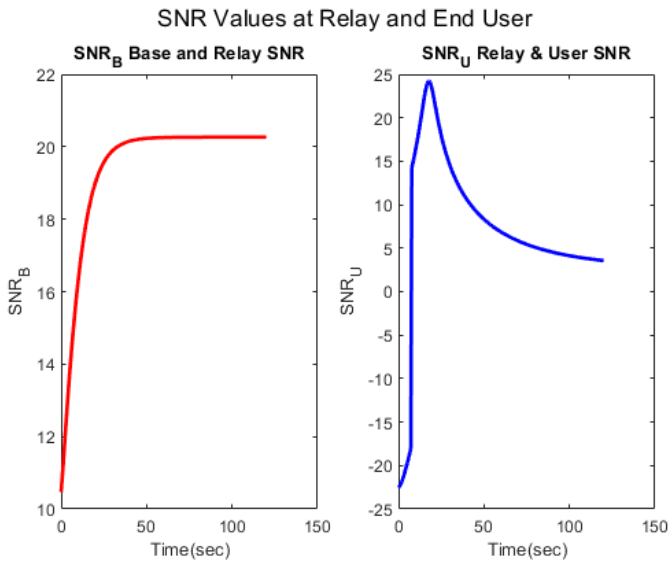

Figure 15 SNR Variation in the UAV pairs

Figure 15 shows the value of the SNR as it varies with time. The SNR value between two pairs of the UAVs is shown. The first pair is the base station and the R-UAV (shown in red). The curve on the right shows the variation in the SNR value between the R-UAV and the UE.

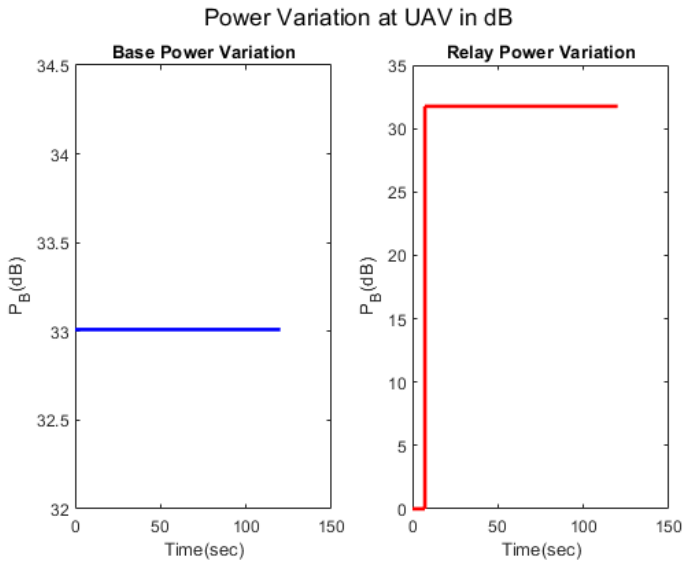

Figure 16 Power value available for Transmission

Figure 16, shows the value of the power available at the base station (left, blue) and the power available for establishing a signal on the R-UAV is shown on the right in red. While the system in a situation where the SNR value between the base station and the R-UAV is under the threshold value for transmission (which is 20dB is this case), the power (in dB) available for the transmission is by the R-UAV 0dB. When the SNR value (refer to figure 15) crosses the threshold value, the power available for transmission at the R-UAV increases accordingly.

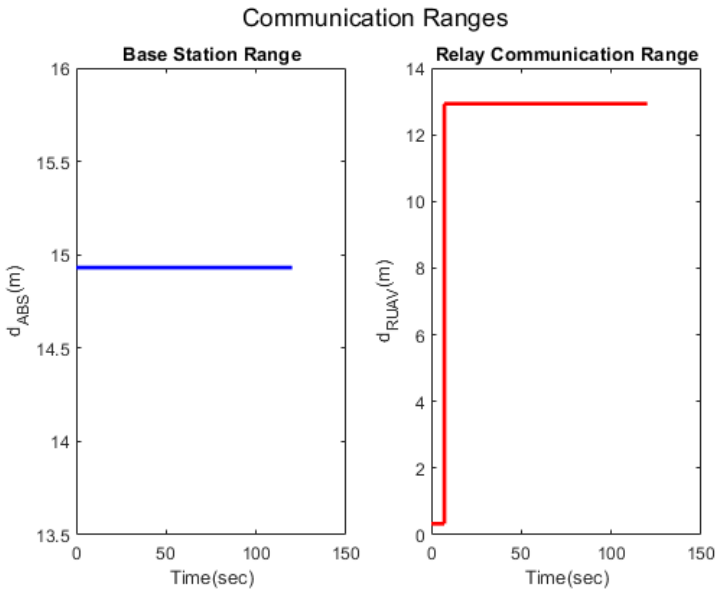

Figure 17 Communication ranges of UAV

Figure 17 shows the range of communication that is similar in nature to the variation in the power available at any given UAV. When the SNR value crosses the threshold value, the increase in the power at the R-UAV is reflected in the range of communication at the same time.

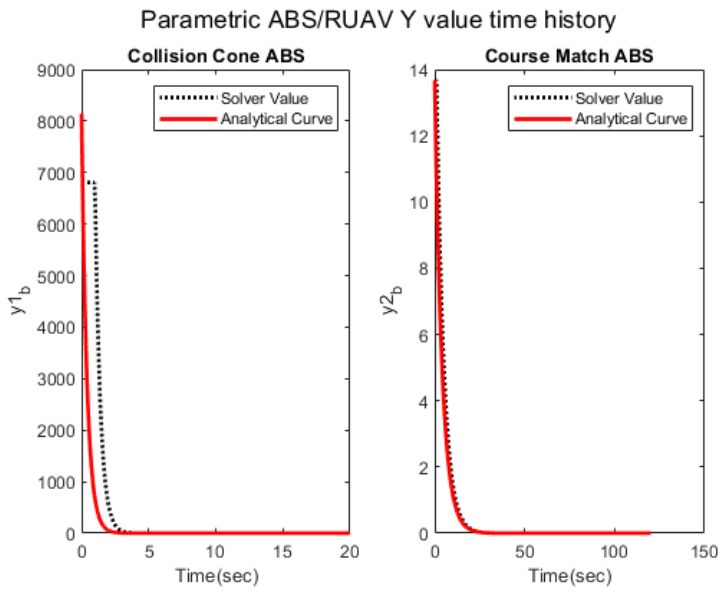

Figure 18 Parameter time history y_1 and y_2

Figure 18 shows the variation of parameters y_1 and y_2 as have been explained in Chapter 3, equations 3.3 and 3.15. The time history of the function follows the changes that are due to application of dynamic inversion as have also been explained in Chapter 3. The decay of the function is guided by a first order ODE and the time constant with which each of these parameter's decay is based on the values of the gains K_1 and K_2 associated with $y_1$and y_2 respectively. The plot on the left shows the decay of the parameter y_1 governing the collision cone function. The plot on the right shows the time history of the parameter y_2, governing the parameter responsible for the course matching of the follower to the leader.

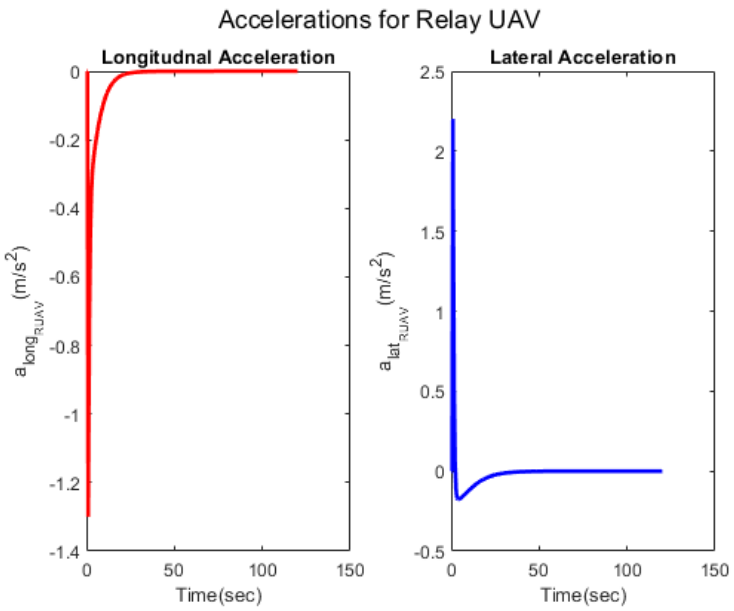

Figure 19 Acceleration Time History of Relay UAV

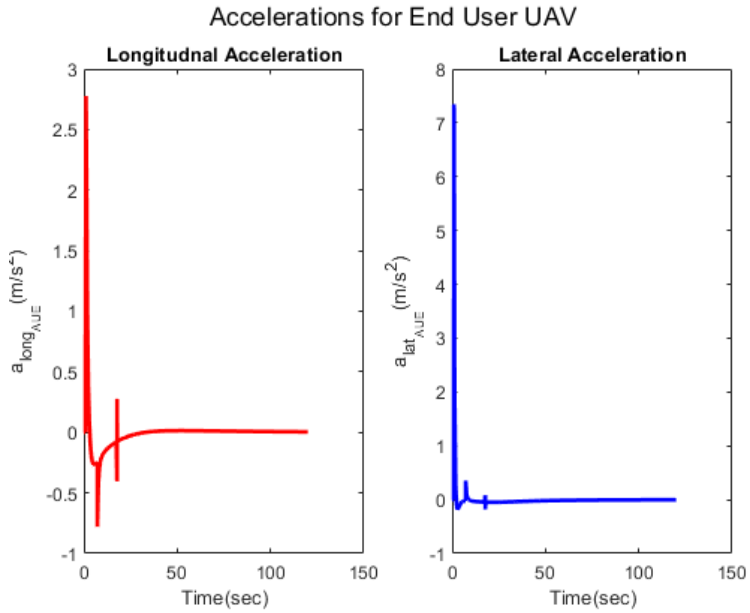

Figure 20 Acceleration Time History of UE UAV

Figures 19 and 20 show the acceleration time history for the relay UAV and the AUE. The left plots in both these figures show the longitudinal acceleration, responsible for change in the speed of the object. The right plots (shown in blue) show the time history of the lateral

acceleration acting on the RUAVs and the UEs, responsible for the change in the direction of movement of the UAVs.

The subsequent simulation plots are along the lines shown in Figure 10 to 20.

4.2 Scenario 2: Collaborative Rendezvous in 5G

Two UAVs head to establish a common link with a base station. In this scenario the RUAV has the guidance law applied to it to work towards lowering the $y_1$and y_2 value with only the base station. The simulation is done in a 5G network condition.

4.2.1 Initial Conditions and Simulation Parameters

Table 4 Scenario 2: Initial Conditions

	Base Station	Relay UAV	End User
Position	(-40,20)	(0,0)	(40,20)
Velocity	0.5 m/s	5 m/s	0.5 m/s
Flight Path Angle	60°	90°	115°
UAV Physical Radius	2m	4m	2m

- ***Base Station Communication Circle Penetration:*** *0 m*
- ***Relay Station Communication Circle Penetration:*** *0 m*
- ***Rendezvous Controller Gain (Relay and Base)*** (K_b) ***:*** *1.5*
- ***Rendezvous Controller Gain (Relay and User)*** (K_u) ***:*** *1*

4.2.2 Communication Conditions

- *Area temperature:* $25\ ^\circ C$
- *Connection Type: 5G Cellular @ 100 MHz bandwidth*
- *Location Type: Free Space*

Table 5 Communication Conditions: Scenario 2

	Base Station	Relay UAV	End User
Power	2W	$Variable$	–
Tx Gain	20dB	20 dB	–
Rx Gain	–	2 dB	2dB

4.2.3 Simulation Results for Scenario 2

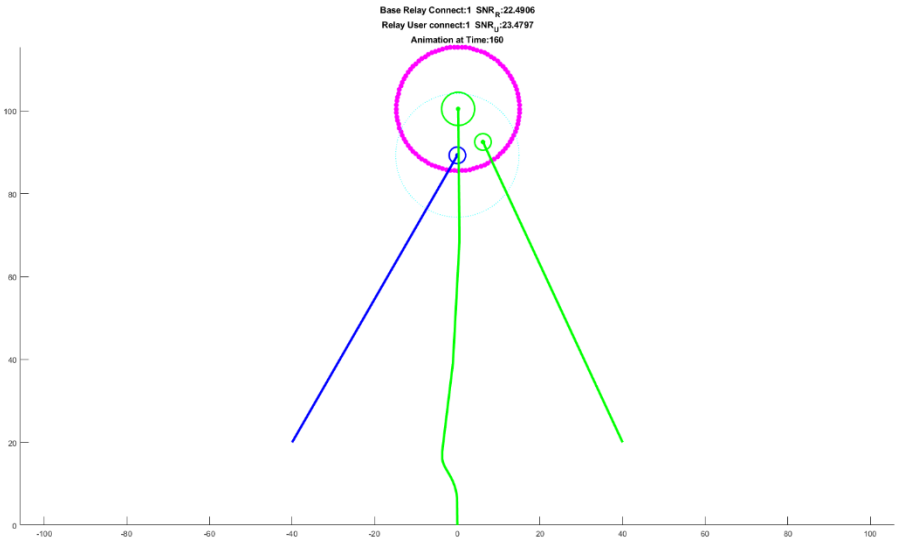

Figure 21 Trajectory plot for Scenario 2

Figure 21 shows the trajectory plot for the movement of the 3 UAVs, this is a collaborative movement where the R-UAV moves through space and uses the parameters y_{1_b} and y_{1_u}, to apply the acceleration such that it is guided to intersect with both the communication circles for the base station and the AUE.

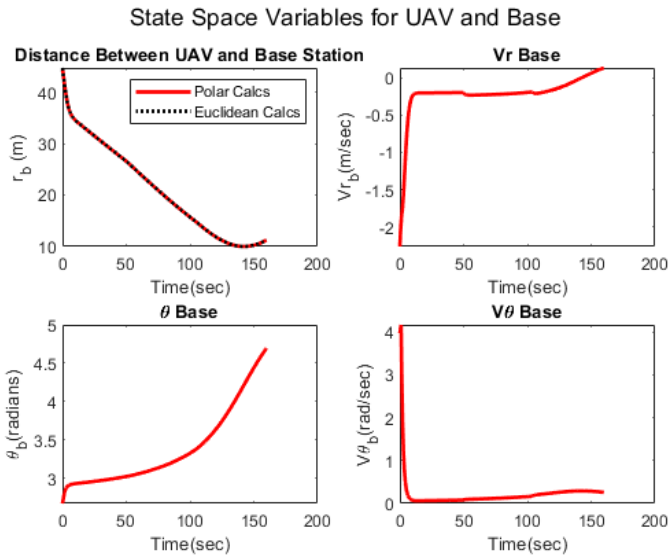

Figure 22 Scenario 2: State Space Time History RUAV and ABS

Figure 22 shows time history for state space for the ABS and R-UAV interaction.

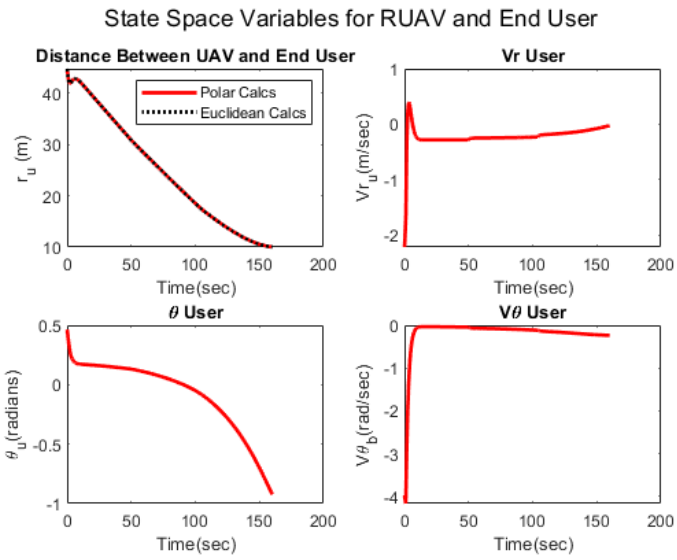

Figure 23 Scenario 2: State Space Time History RUAV and UE

Figure 23 shows time history for state space for the R-UAV and AUE interaction.

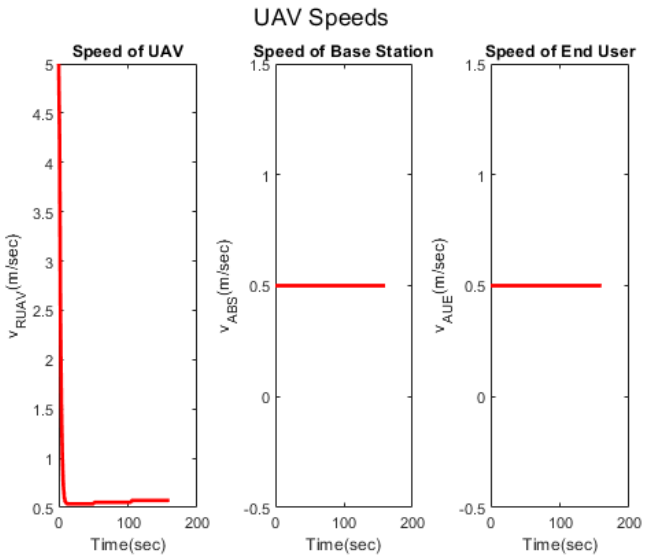

Figure 24 Scenario 2: Speed Time History for RUAV, ABS, and UE

Figure 24 shows time history for speeds for the 3 UAVs.

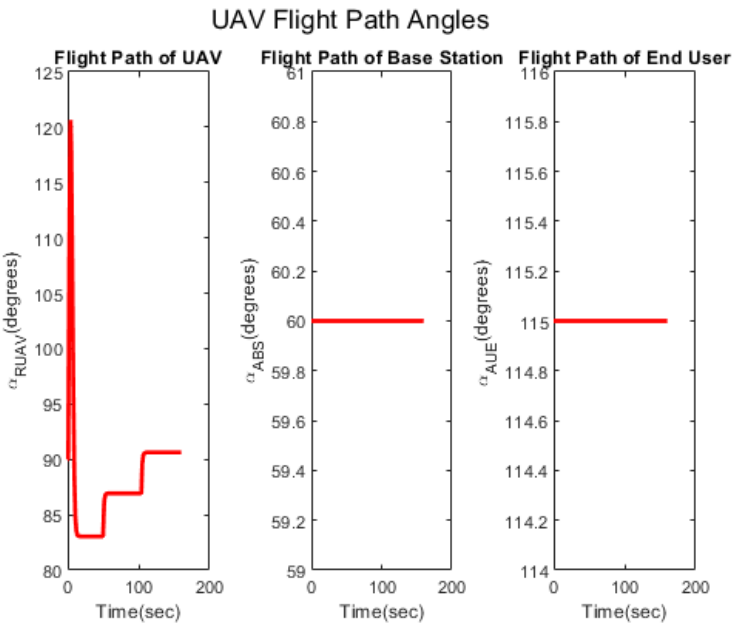

Figure 25 Scenario 2: Flight Path Angle Time History for RUAV, ABS, and UE

Figure 25 shows time history for flight path angles for the 3 UAVs.

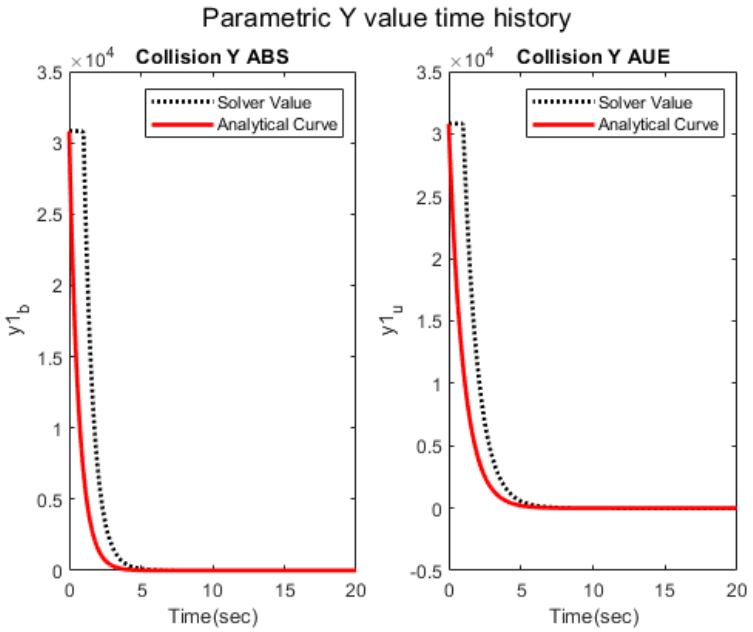

Figure 26 Parametric Dynamic Inversion decay for Collision Cone between RUAV and ABS and UE (left to right)

Figure 26 shows the decay of parametric values y_{1_b} and y_{1_u} as a time history plot.

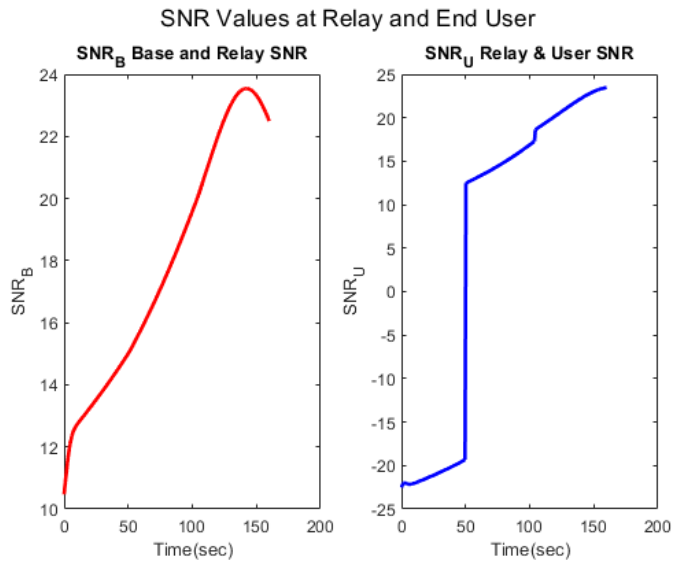

Figure 27 SNR Variation in the UAV pairs

Figure 27 shows the time history plot of the SNR_B (signal to noise ratio for base station and relay interaction) and SNR_U (signal to noise ratio for R-UAV and AUE interaction).

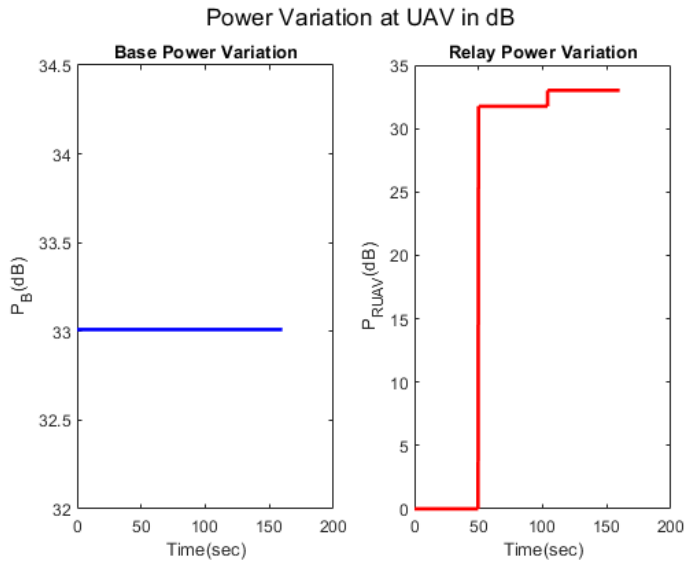

Figure 28 Power value available for Transmission

Figure 28 shows the time history plot of the power available for transmission at the base station and the R-UAV.

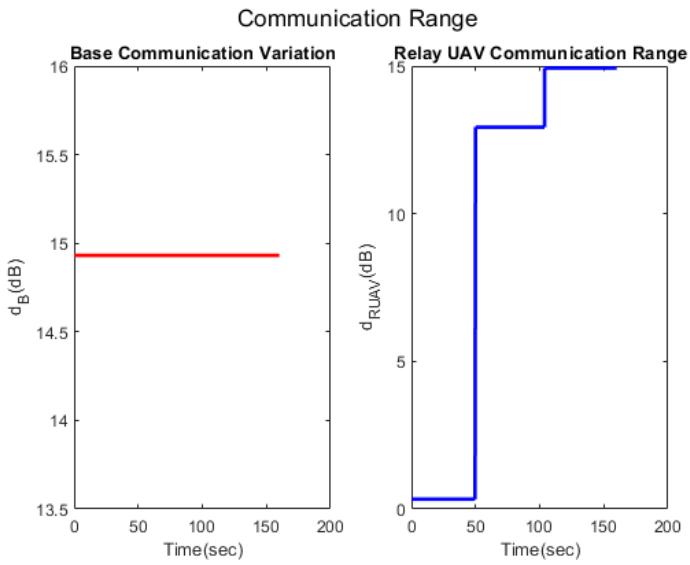

Figure 29 Communication Range of ABS and RUAV

Figure 29 shows the time history plot of the communication of the base station and the R-UAV.

4.3 Scenario 3: Chain Link in Wi-Fi 5

In this scenario, the communication occurs through Wi-Fi 5. The variation in the power, SNR along with other parameters affecting the communication between the objects is shown below.

4.3.1 Initial Conditions and Simulation Conditions

Table 6 Scenario 3: Initial Conditions

	Base Station	Relay UAV	End User
Position	(-160,80)	(0,0)	(160,80)
Velocity	2m	5m	2m
Flight Path Angle	60°	100°	115°
UAV Physical Radius	2m	4m	2m

- ***Relay Station Communication Circle Penetration:*** *5m*
- ***Base Station Communication Circle Penetration:*** *5m*
- ***Rendezvous Controller Gain (Relay and Base)*** (K_{1b}) *: 2.5*
- ***Course Match Controller Gain (Relay and Base)*** (K_{2b})*: 0.045*
- ***Rendezvous Controller Gain (Relay and User)*** (K_{1u}) *: 2.5*

- ***Course Match Controller Gain (Relay and User)*** (K_{2u}) *: 0.035*

4.3.2 Communication Conditions

- *Area temperature:* 25 ° *C*
- *Connection Type: Wi-Fi 5 @ 160 MHz bandwidth*
- *Location Type: Free Space*

Table 7 Communication Conditions: Scenario 2

	Base Station	Relay UAV	End User
Power	2W	*Variable*	–
Tx Gain	20dB	20 dB	–
Rx Gain	–	2 dB	2dB

4.3.3 Simulation Results for Scenario 3

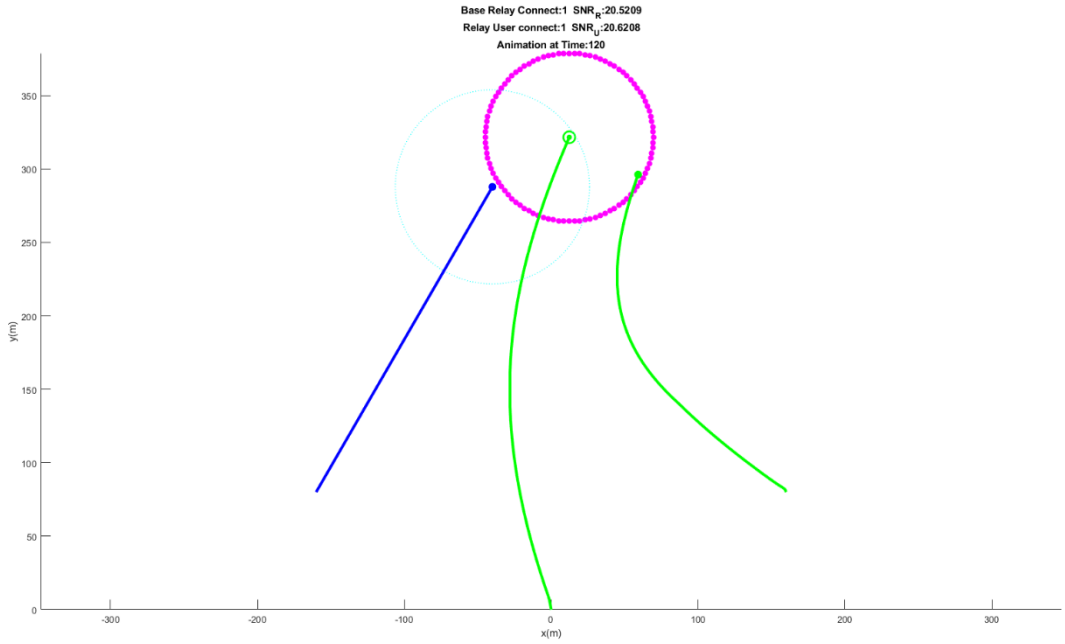

Figure 30 Trajectory plot for Scenario 3

In this scenario the relay is being guided as the follower to the ABS and the AUE is guided by its laws to follow the RUAV in turn, the motion is thus that of a leader-follower type as shown in Figure 30 above.

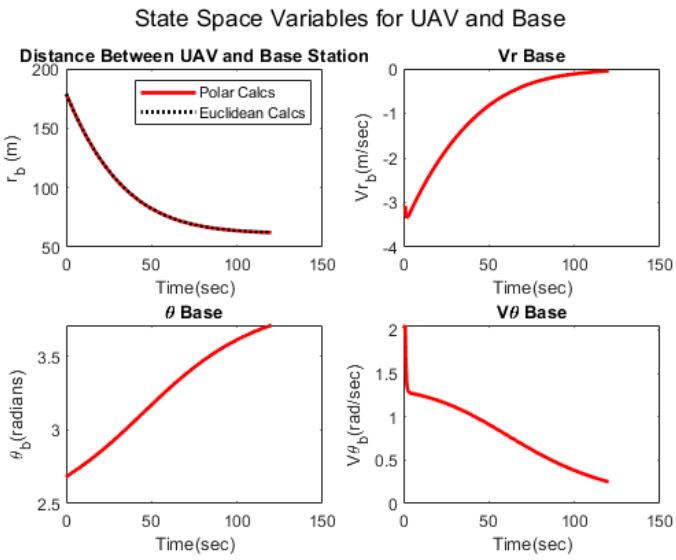

Figure 31 Scenario 3: State Space Time History RUAV and ABS

Figure 31 shows time history for state space for the ABS and R-UAV interaction.

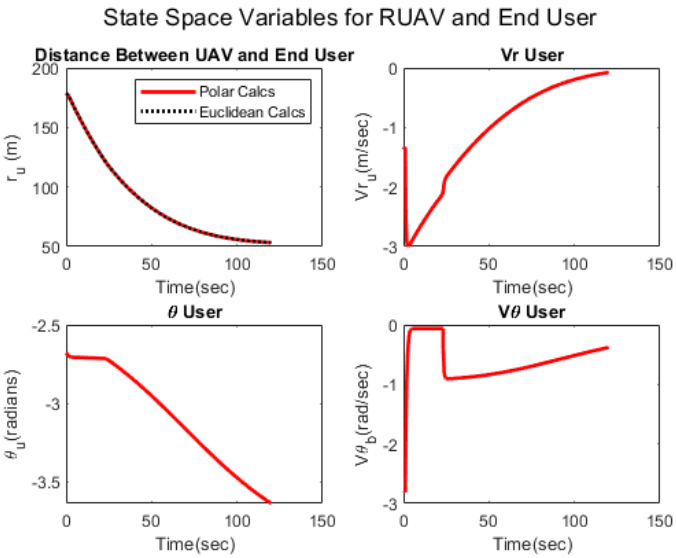

Figure 32 Scenario 3: State Space Time History RUAV and UE

Figure 32 shows time history for state space for the R-UAV and AUE interaction.

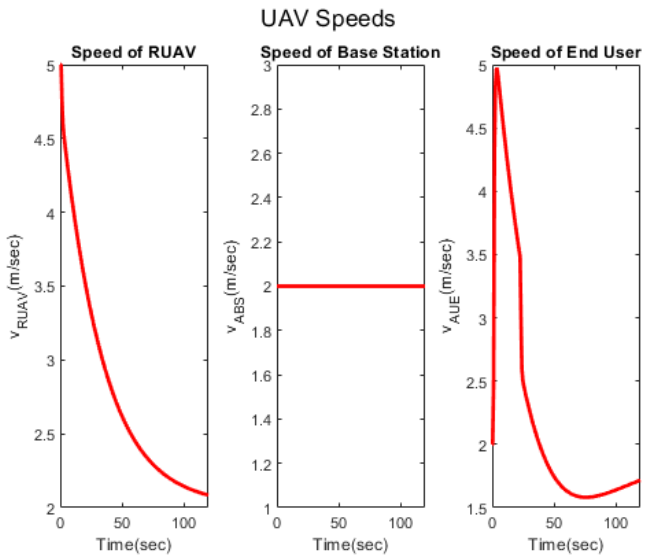

Figure 33 Scenario 3: Speed Time History for RUAV, ABS, and UE

Figure 33 shows time history for speeds for the 3 UAVs.

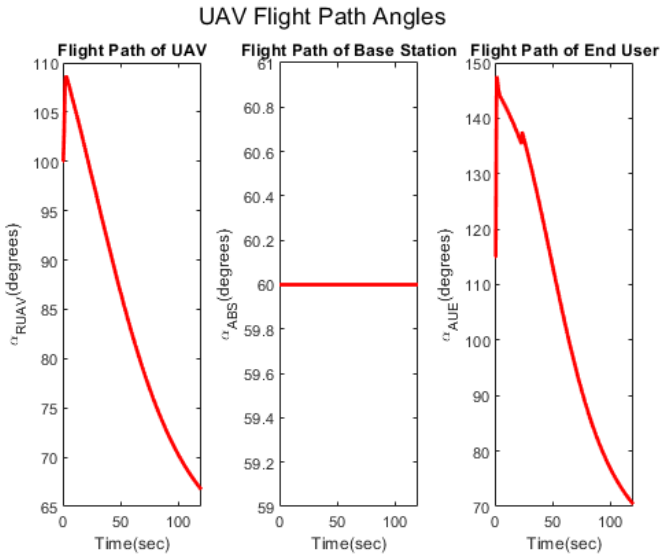

Figure 34 Scenario 3: Flight Path Angle Time History for RUAV, ABS, and UE

Figure 34 shows time history for flight path angles for the 3 UAVs.

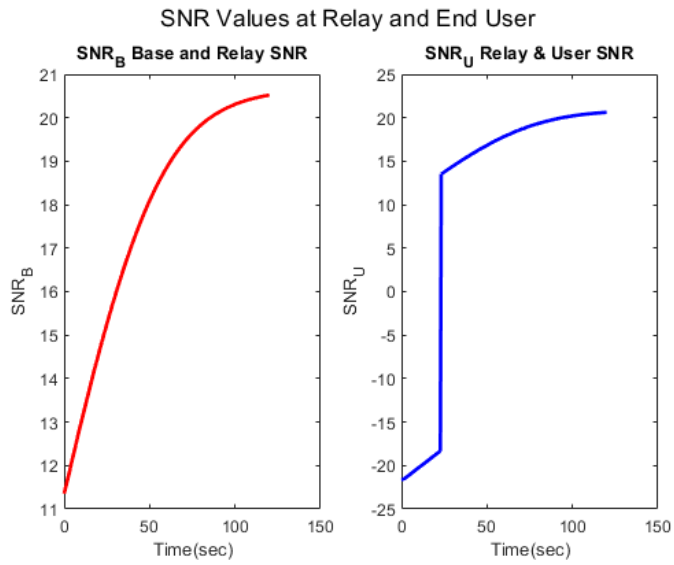

Figure 35 SNR Variation in the UAV pairs

Figure 35 shows the time history plot of the SNR_B (signal to noise ratio for base station and relay interaction) and SNR_U (signal to noise ratio for R-UAV and AUE interaction).

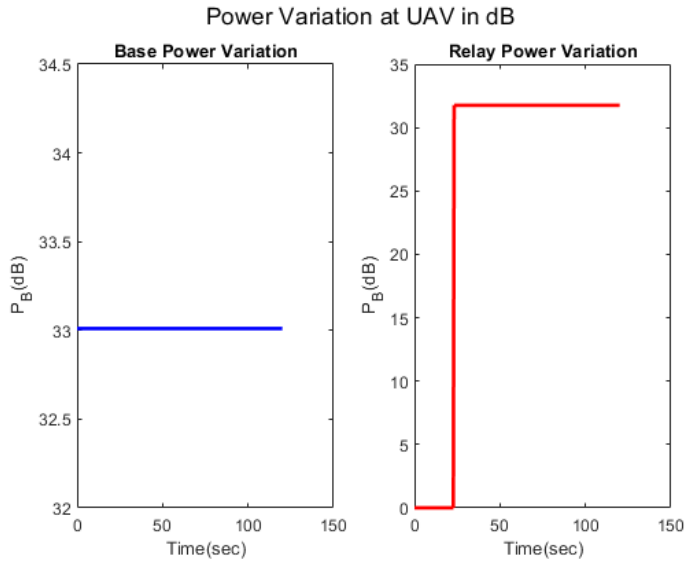

Figure 36 Power value available for Transmission

Figure 36 shows the time history plot of the power available for transmission at the ABS and the R-UAV

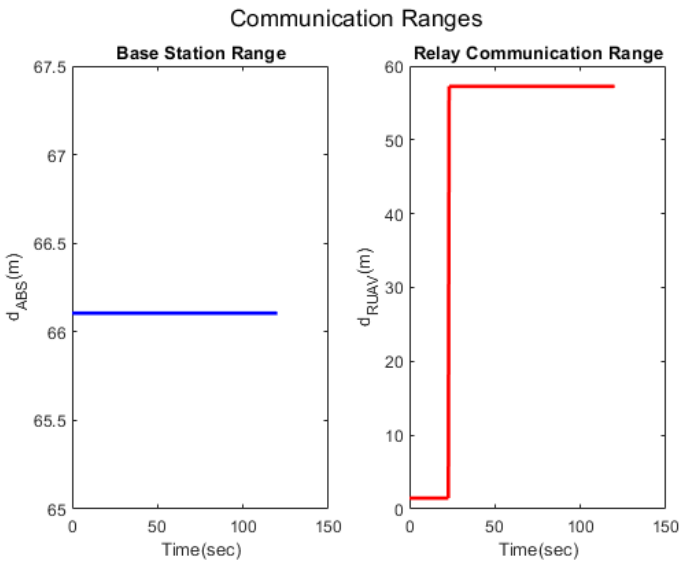

Figure 37 Communication Range of ABS and RUAV

Figure 37 shows the time history plot of the communication of the base station and the R-UAV.

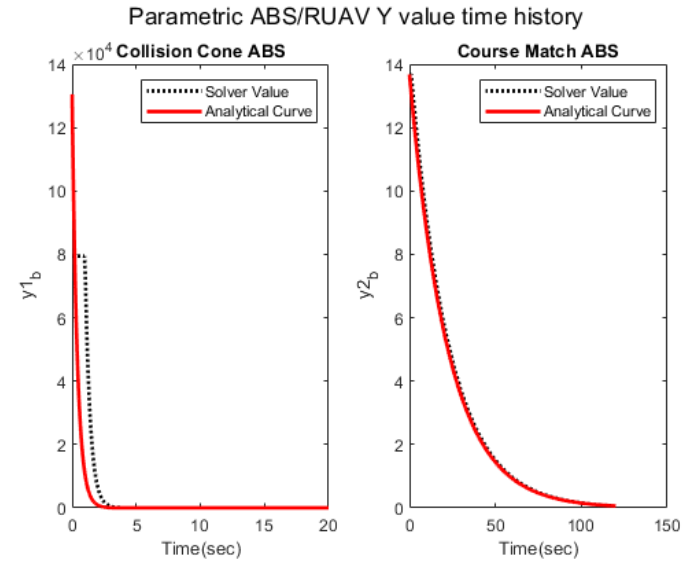

Figure 38 Parametric Dynamic Inversion decay y_1 and y_2 RUAV and ABS

Figure 38 shows the decay of parametric values y_{1_b} and y_{2_b} as a time history plot.

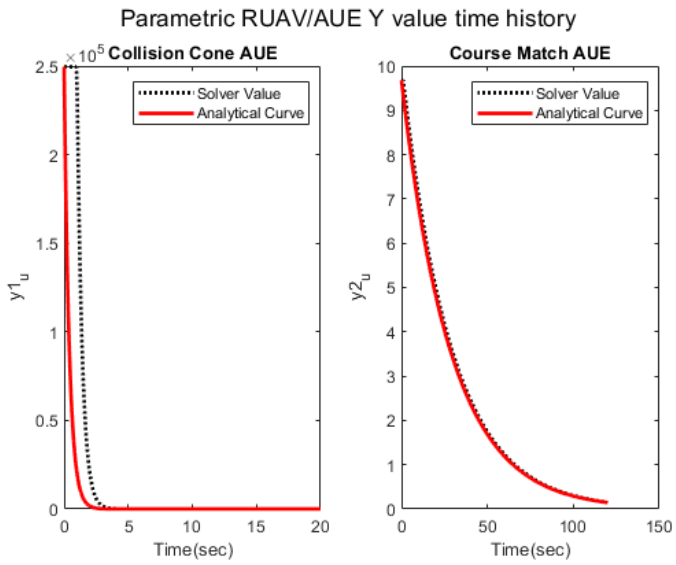

Figure 39 Parametric Dynamic Inversion decay y_1 and y_2 RUAV and UE

Figure 38 shows the decay of parametric values y_{1_u} and y_{2_u} as a time history plot.

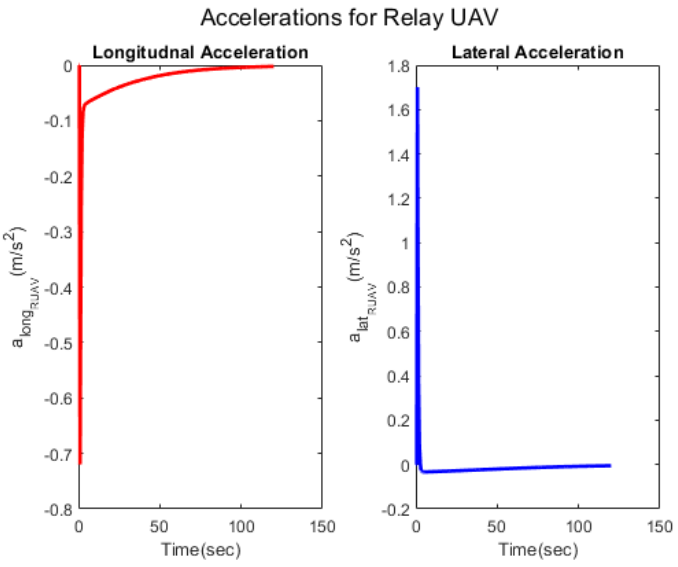

Figure 40 Acceleration Time History for Relay UAV

Figure 40 shows longitudinal and lateral acceleration for the R-UAV.

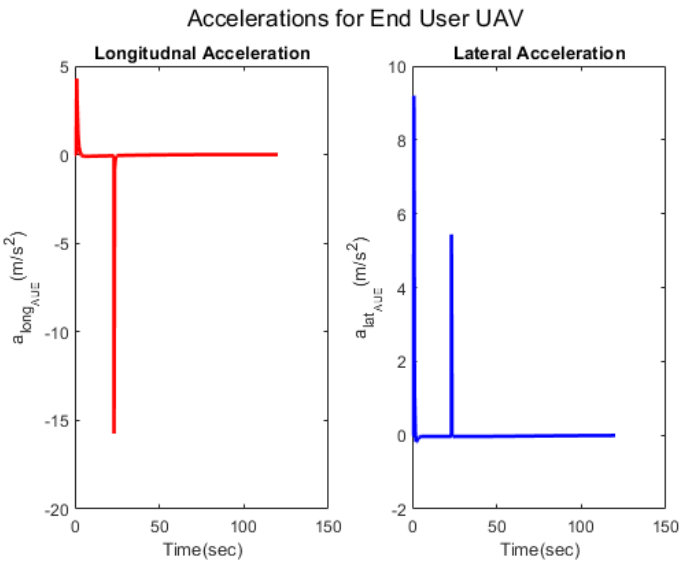

Figure 41 Acceleration Time History for UE UAV

Figure 41 shows longitudinal and lateral acceleration for the AUE.

4.4 Scenario 4: Collaborative Rendezvous in Wi-Fi 5

Two UAVs head to establish a common link with a base station. In this scenario the RUAV has the guidance law applied to it to work towards lowering the $y_1$and y_2 value with only the base station. The simulation is done in a Wi-Fi 5 network condition.

4.4.1 Initial Conditions and Simulation Conditions

Table 8 Scenario 4: Initial Conditions

	Base Station	Relay UAV	End User
Position	(-160,80)	(0,0)	(160,80)
Velocity	2 m/s	10 m/s	2 m/s
Flight Path Angle	60°	90°	115°
UAV Physical Radius	2m	4m	2m

- ***Base Station Communication Circle Penetration:*** $0m$
- ***Relay Station Communication Circle Penetration:*** $0m$
- ***Rendezvous Controller Gain (Relay and Base)*** (K_b) *:2.5*

- ***Rendezvous Controller Gain (Relay and User)*** (K_u) *: 1*

4.4.2 Communication Conditions

- *Area temperature:* 25 ° *C*
- *Connection Type: Wi-Fi 5 @ 160 MHz bandwidth*
- *Location Type: Free Space*

Table 9 Communication Conditions: Scenario 4

	Base Station	Relay UAV	End User
Power	2W	$Variable$	–
Tx Gain	20dB	20 dB	–
Rx Gain	–	2 dB	2dB

4.4.3 Simulation Results for Scenario 4

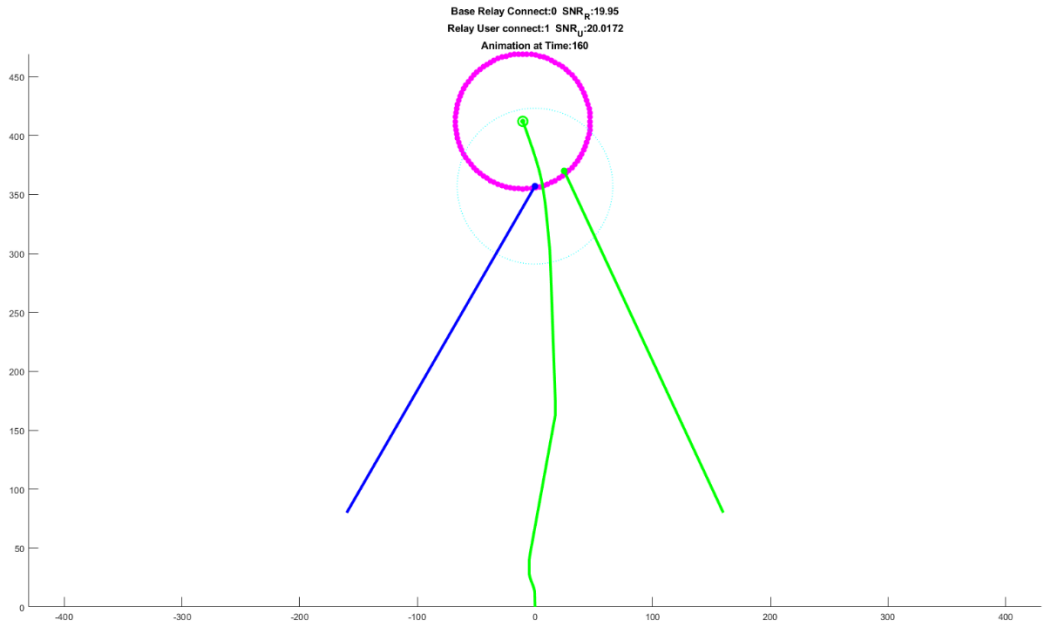

Figure 42 Trajectory plot for Scenario 4

The trajectory in Figure 42 plot shows collaborative rendezvous guidance laws acting on the R-UAV, the ABS and AUE are moving in straight line and the R-UAV is moving to bridge the gap between the ABS and the AUE.

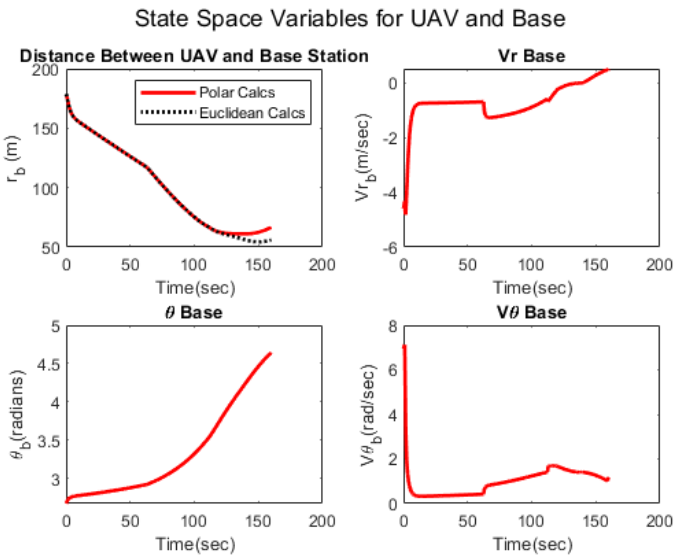

Figure 43 Scenario 4: State Space Time History RUAV and ABS

Figure 43 shows time history for state space for the ABS and R-UAV interaction.

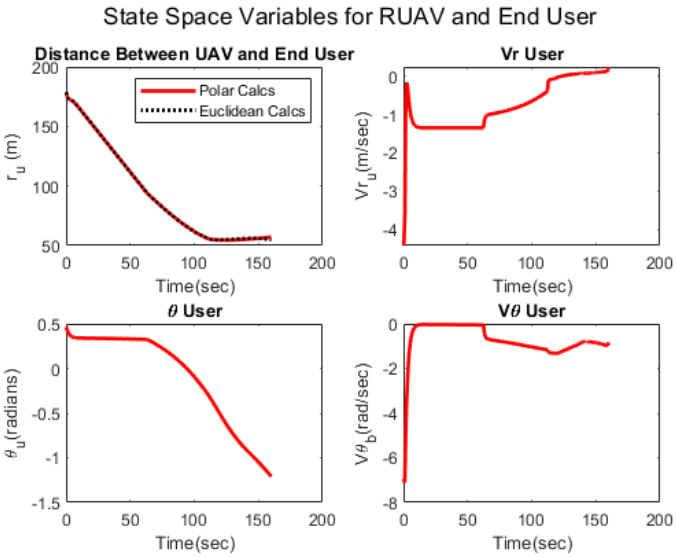

Figure 44 Scenario 4: State Space Time History RUAV and UE

Figure 44 shows time history for state space for the R-UAV and AUE interaction.

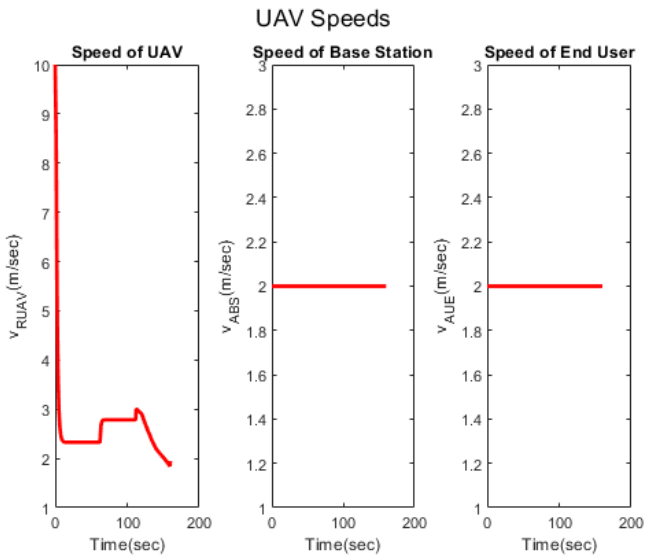

Figure 45 Scenario 4: Speed Time History for RUAV, ABS, and UE

Figure 45 shows time history for speeds for the 3 UAVs.

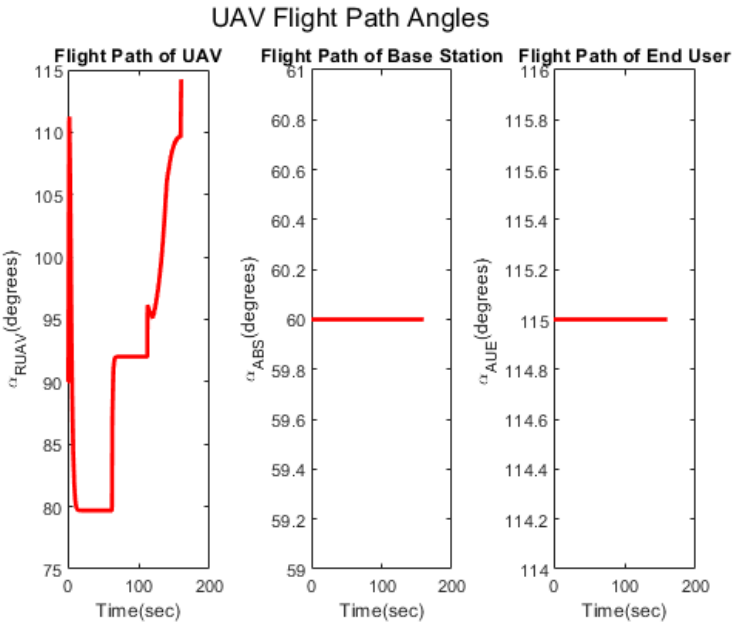

Figure 46 Scenario 4: Flight Path Angle Time History for RUAV, ABS, and UE

Figure 46 shows time history for flight path angles for the 3 UAVs.

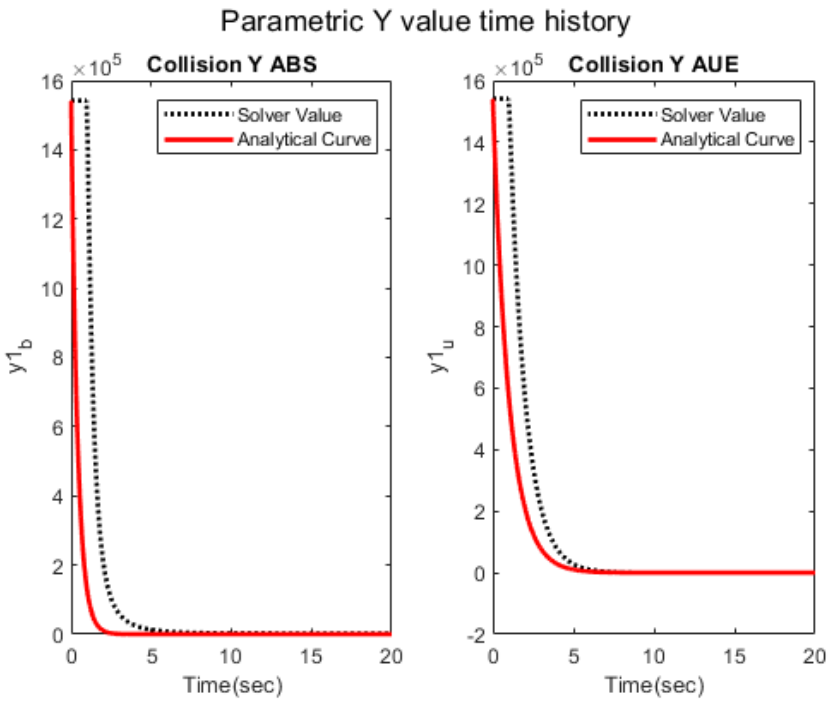

Figure 47 Parametric Dynamic Inversion decay for Collision Cone between RUAV and ABS and UE (left to right)

Figure 47 shows the decay of parametric values y_{1_b} and y_{1_u} as a time history plot.

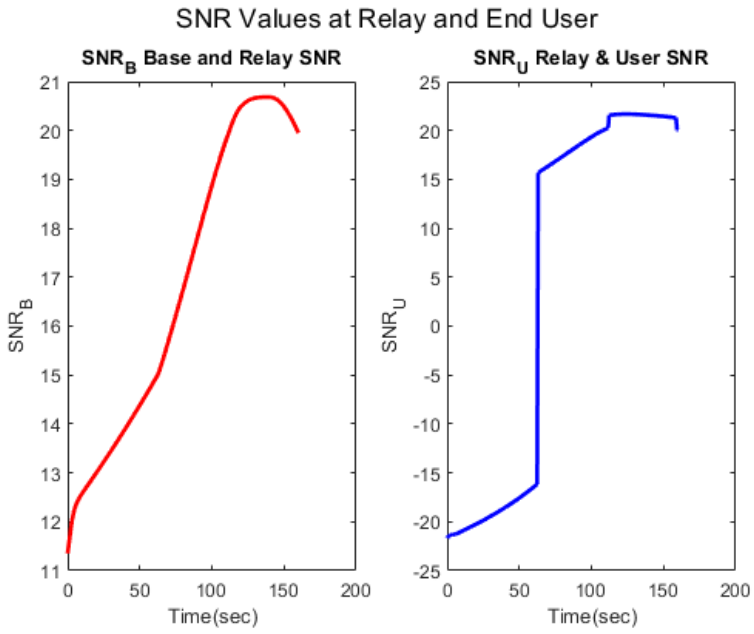

Figure 48 SNR Variation in the UAV pairs

Figure 48 shows the time history plot of the SNR_B (signal to noise ratio for base station and relay interaction) and SNR_U (signal to noise ratio for R-UAV and AUE interaction).

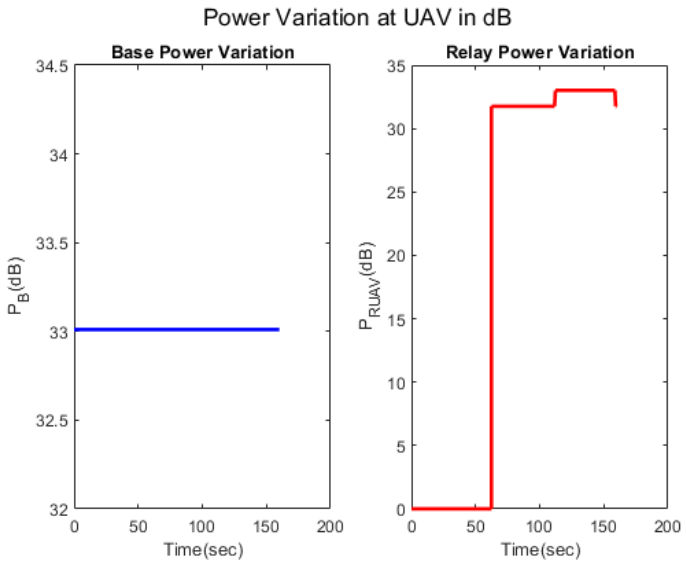

Figure 49 Power value available for Transmission

Figure 49 shows the time history plot of the power available for transmission at the ABS and the R-UAV

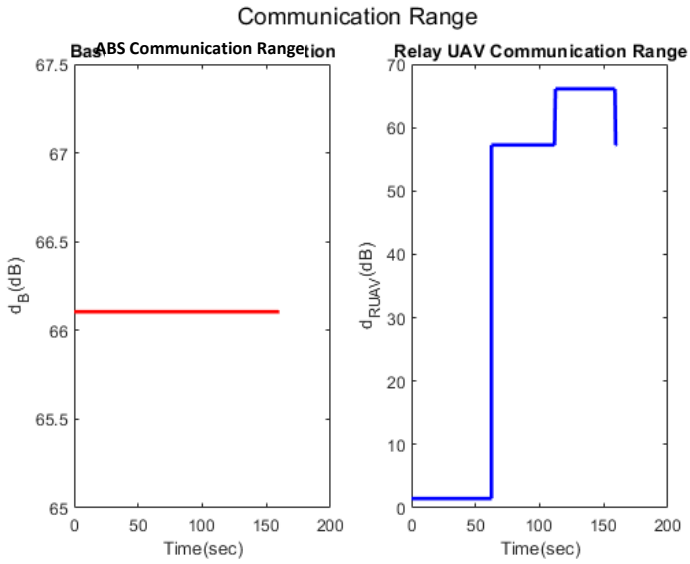

Figure 50 Communication Range of ABS and RUAV

Figure 50 shows the time history plot of the communication of the base station and the R-UAV.

4.5 Scenario 5: Collaborative Rendezvous in Wi-Fi for 3 User

To showcase the working of the multi-user interface in a 2-user and 3-user simulation has been performed, below shown is a 3-user simulation and its results.

4.5.1 Initial Conditions and Simulation Conditions

Table 10 Scenario 5: Initial Conditions

	Base Station	Relay UAV	User 1	User 2	User 3
Position (x, y) in (m)	(-160,80)	(0,0)	(160,80)	(240,120)	(280,130)
Velocity(m/s)	2	10	2	2.5	2.5
Flight Path Angle (deg)	60	90	115	120	110
UAV Physical Radius (m)	2m	4m	2m	2	2

- ***Base Station Communication Circle Penetration:*** *5m*
- ***Relay Station Communication Circle Penetration:*** *5m*
- ***User 1 Communication Circle Penetration:*** *5m*
- ***User 2 Communication Circle Penetration:*** *5m*
- ***Rendezvous Controller Gain (Relay and Base)*** (K_{1_b}) ***:*** *4.5*
- ***Alignment Controller Gain (Relay and Base)*** (K_{2_b}) ***:*** *0.045*
- ***Rendezvous Controller Gain (Relay and User 1)*** $(K_{1_{u1a}})$ ***:*** *2.5*
- ***Alignment Controller Gain (Relay and User 1)*** $(K_{2_{u1a}})$ ***:*** *0.035*
- ***Rendezvous Controller Gain (User 1 and User 2)*** $(K_{1_{u12}})$ ***:*** *3.5*
- ***Alignment Controller Gain (User 1 and User 2)*** $(K_{2_{u12}})$ ***:*** *0.015*
- ***Rendezvous Controller Gain (User 2 and User 3)*** $(K_{1_{u23}})$ ***:*** *5.5*
- ***Alignment Controller Gain (User 2 and User 3)*** $(K_{2_{u23}})$ ***:*** *0.005*

4.5.2 Communication Conditions

- *Area temperature:* $25\ ^\circ C$
- *Connection Type: Wi-Fi 5 @ 160 MHz bandwidth*

- *Location Type: Free Space*

Table 11 Scenario 5: Communication Conditions

	Base Station	Relay UAV	User 1	User 2	User 3
Power	2W	$Variable$	$Variable$	$Variable$	$Variable$
Tx Gain	20dB	20 dB	20 dB	20 dB	–
Rx Gain	–	2 dB	2dB	2dB	2dB

4.5.3 Simulation Results for Scenario 5

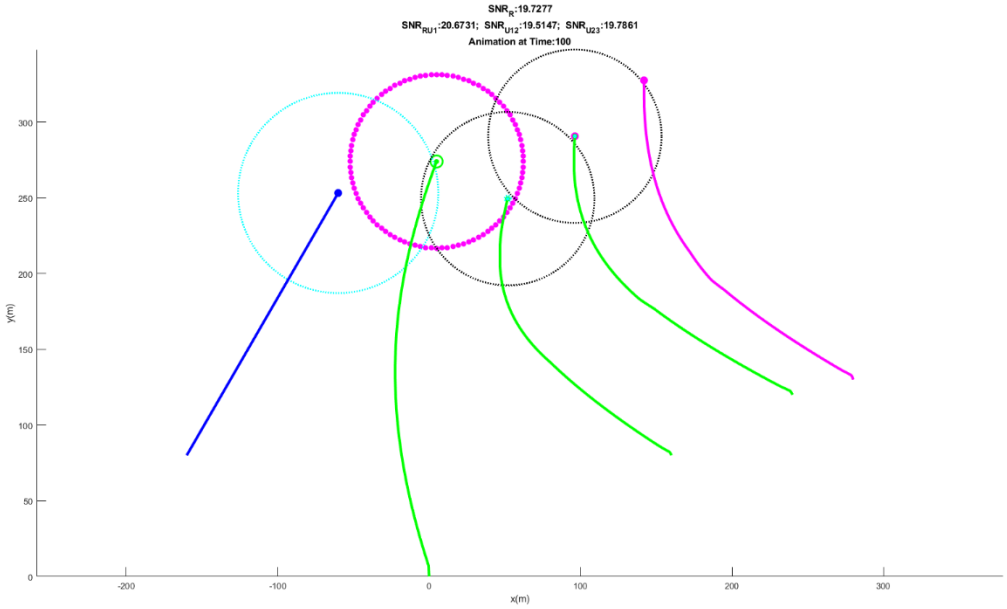

Figure 51 Multi-UAV Leader Follower trajectory Plot

Simulation result in Figure 51 shows an n-UAV system with each AUE acting as a follower to the AUE that is subsequently following another UAV. The base station is the leader for the pack, followed by the R-UAV, the first UAV follows R-UAV, followed by the second AUE, and so on.

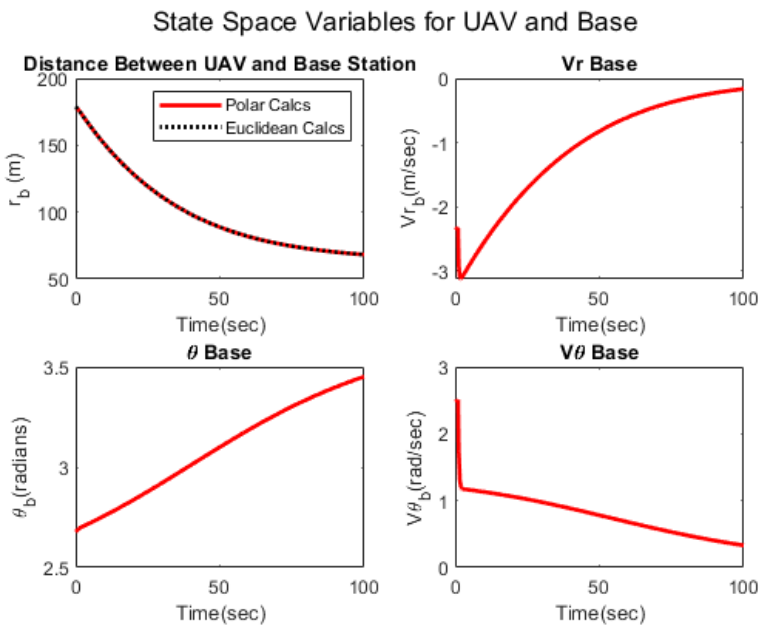

Figure 52 State Space time history: RUAV and ABS

Figure 52 shows time history for state space for the ABS and R-UAV interaction.

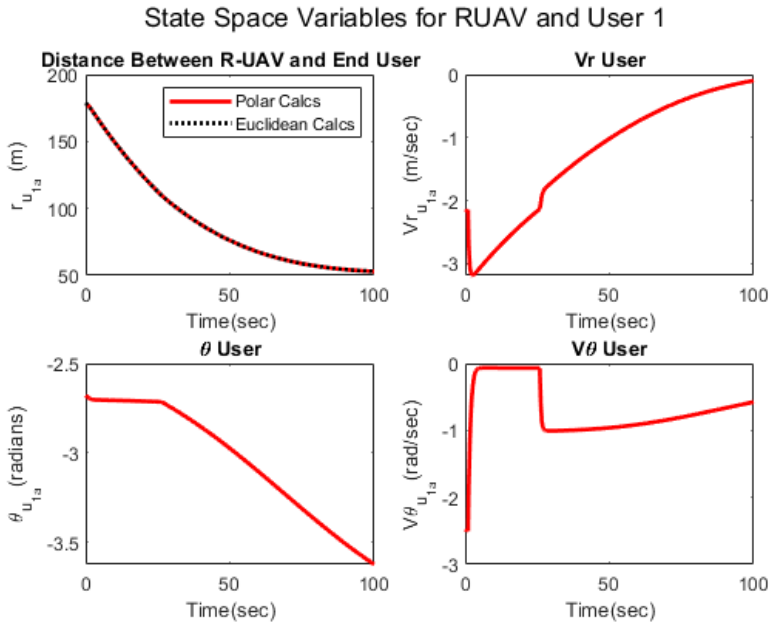

Figure 53 State Space time history: RUAV and UE1

Figure 53 shows time history for state space for the R-UAV and AUE1 interaction.

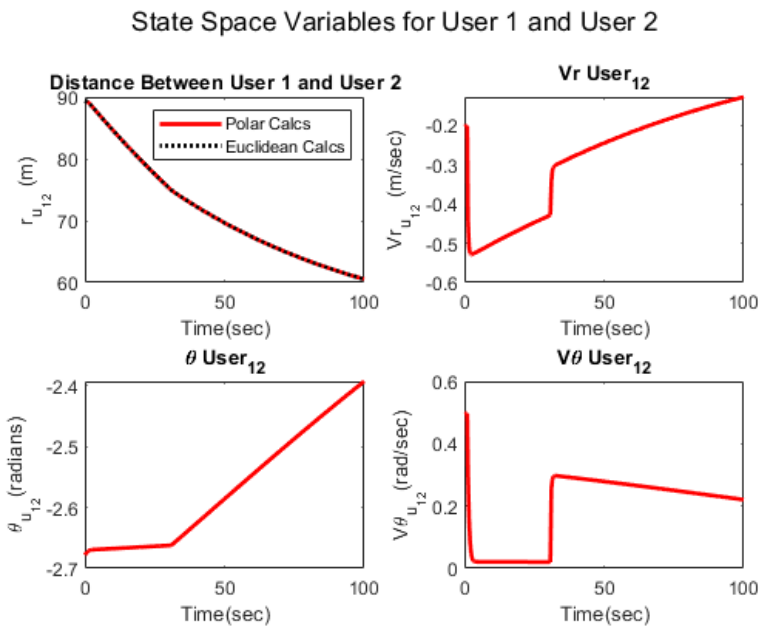

Figure 54 State Space time history: UE1 and UE2

Figure 54 shows time history for state space for the AUE1 and AUE2 interaction.

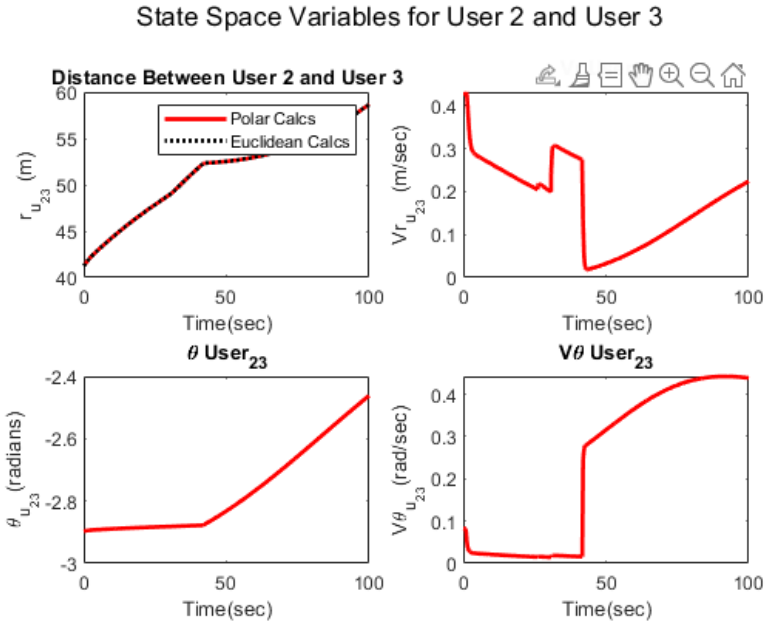

Figure 55 State Space time history: UE2 and UE3

Figure 55 shows time history for state space for the AUE2 and AUE3 interaction.

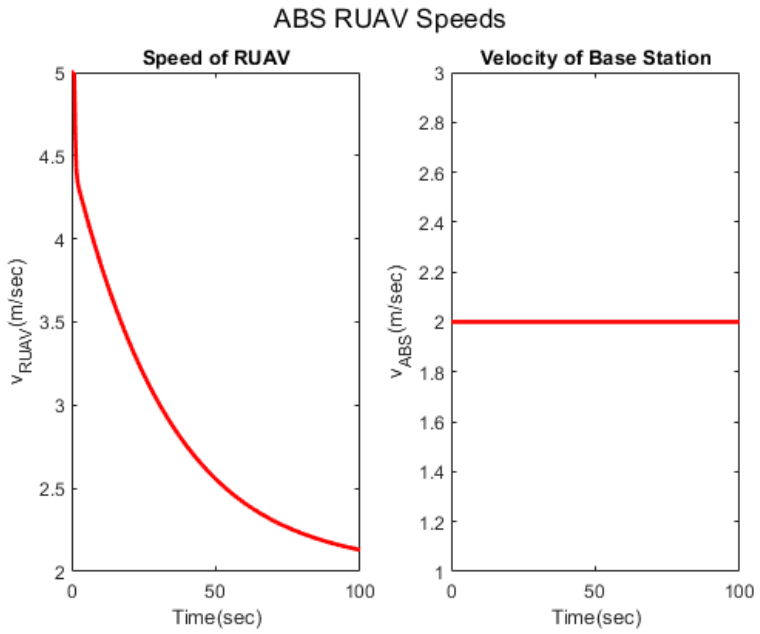

Figure 56 Speed time history: ABS and RUAV

Figure 56 shows time history for speeds for the R-UAV and ABS.

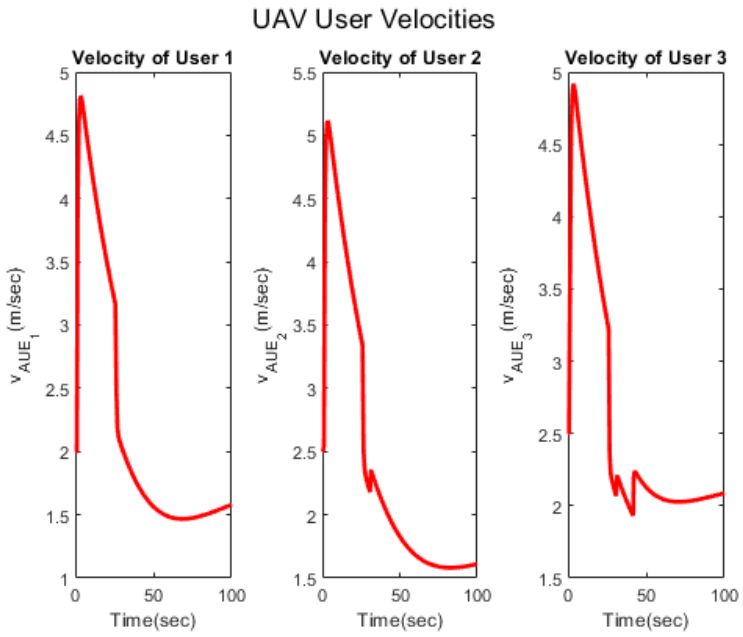

Figure 57 Speed time history: UE: 1,2, and 3

Figure 57 shows time history for speeds for the AUE 1,2, and 3.

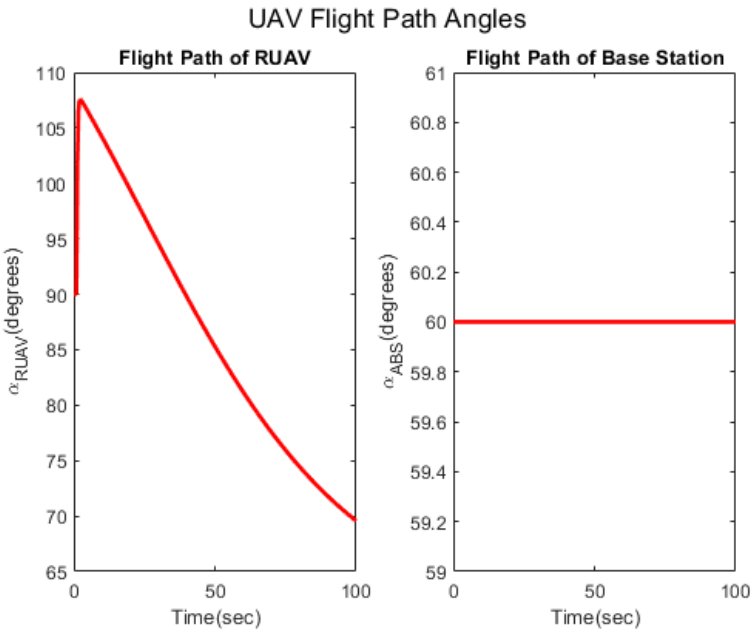

Figure 58 Flight Path time history: ABS and RUAV

Figure 58 shows time history for flight path angle for the R-UAV and ABS.

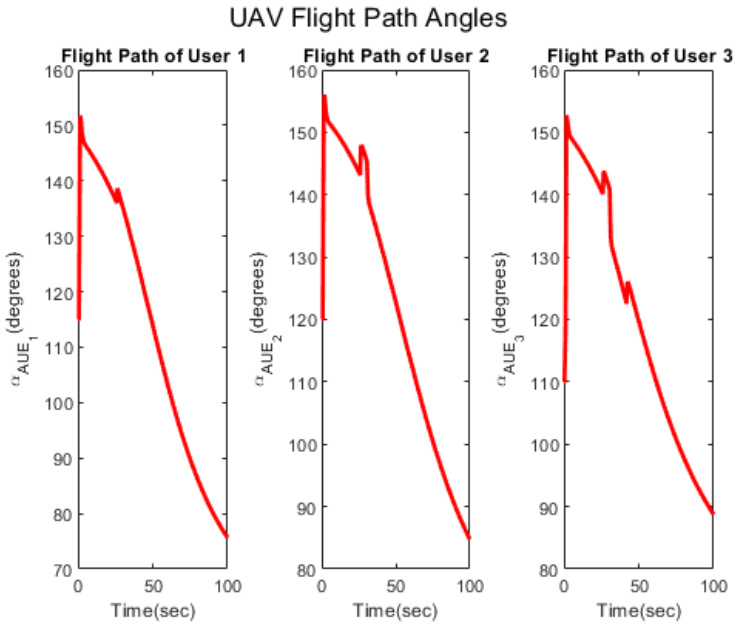

Figure 59 Figure 55 Speed time history: UE 1,2, & 3

Figure 59 shows time history for flight path angle for the AUE 1,2, and 3.

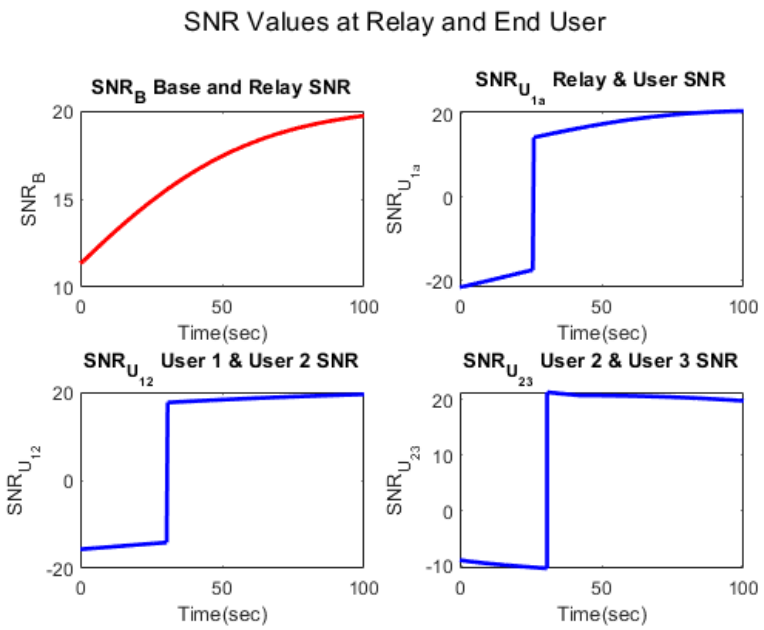

Figure 60 SNR time history

Figure 60 shows the time history plot of the SNR_B (signal to noise ratio for base station and relay interaction), $SNR_{U_{1a}}$ (signal to noise ratio for R-UAV and AUE1 interaction), $SNR_{U_{12}}$ (signal to noise ratio for AUE1 and AUE2 interaction), $SNR_{U_{23}}$ (signal to noise ratio for AUE2 and AUE3 interaction)

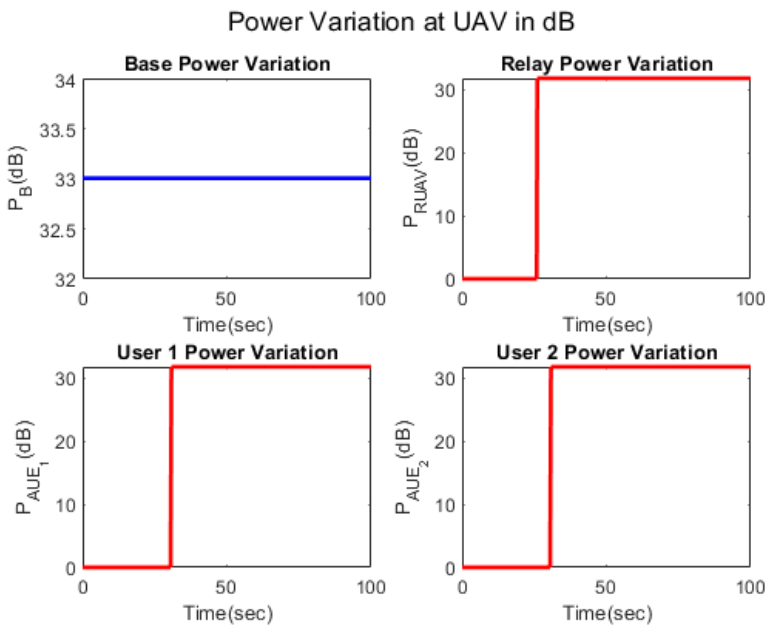

Figure 61 Available power at various UAVs time history

Figure 61 shows the time history plot of the power available at ABS, R-UAV, and AUE 1,2, and 3.

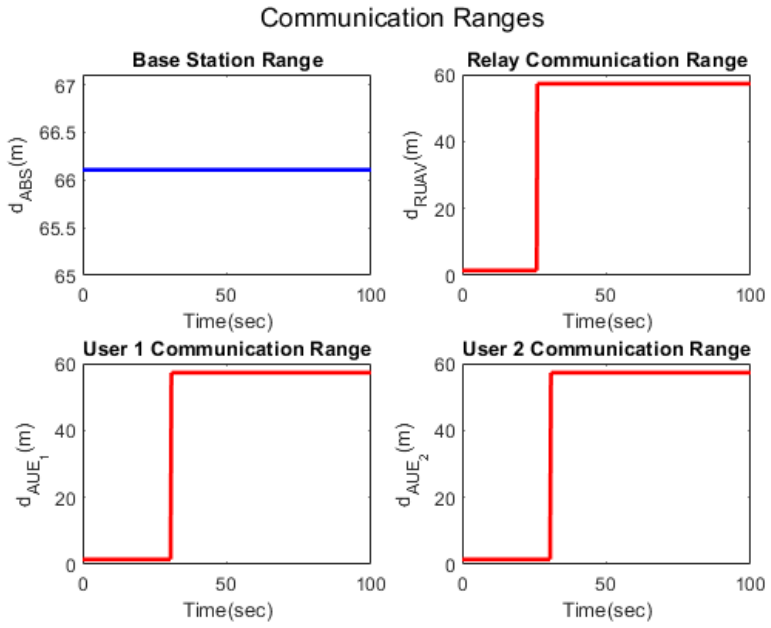

Figure 62 Communication Range Variation time history

Figure 62 shows the time history plot of the communication of the ABS, the R-UAV, and AUEs 1,2, and 3.

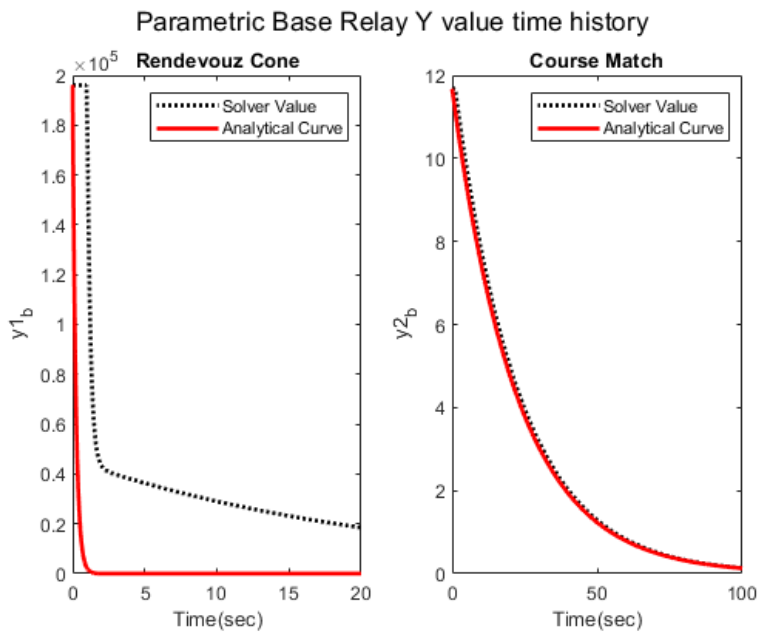

Figure 63 y_1 and y_2 time history ABS and RUAV

Figure 63 shows the decay of parametric values y_{1_b} and y_{2_b} as a time history plot.

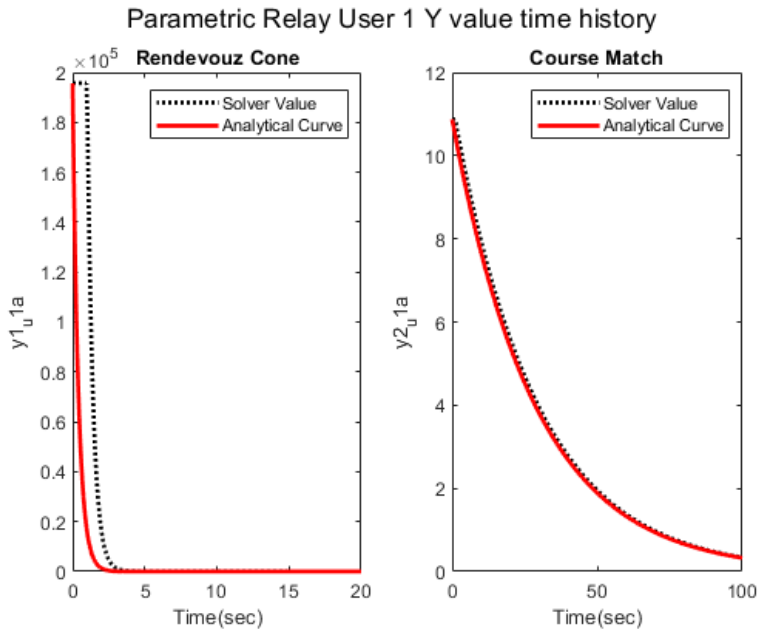

Figure 64 y_1 and y_2 time history RUAV & UE1

Figure 64 shows the decay of parametric values $y_{1_{1u}}$ and $y_{2_{1u}}$ as a time history plot.

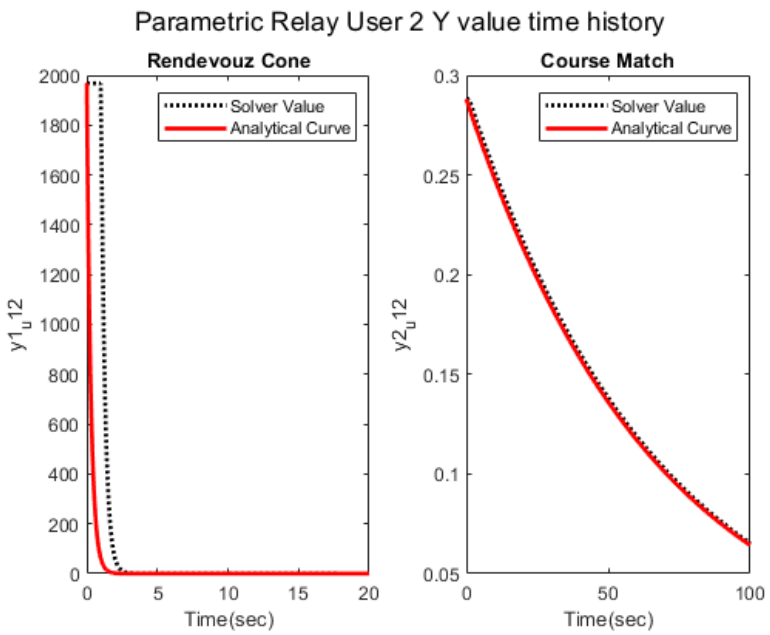

Figure 65 y_1 and y_2 time history UE1 and UE2

Figure 65 shows the decay of parametric values $y_{1_{12}}$ and $y_{2_{12}}$ as a time history plot.

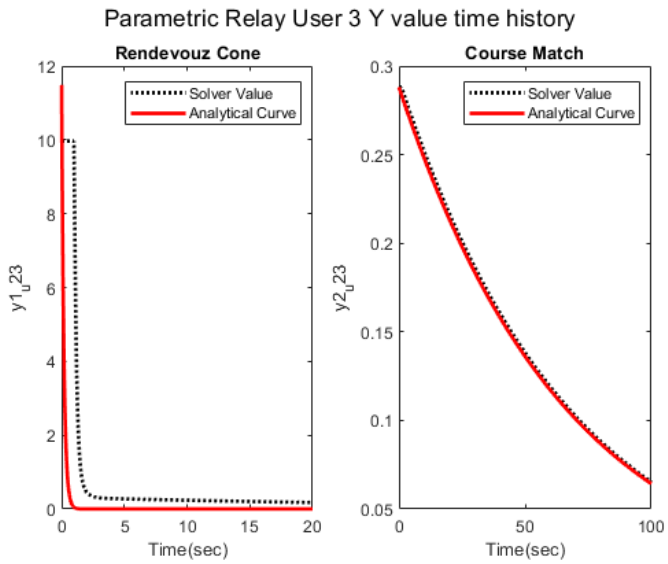

Figure 66 y_1 and y_2 time history UE2 and UE3

Figure 63 shows the decay of parametric values $y_{1_{23}}$ and $y_{2_{23}}$ as a time history plot.

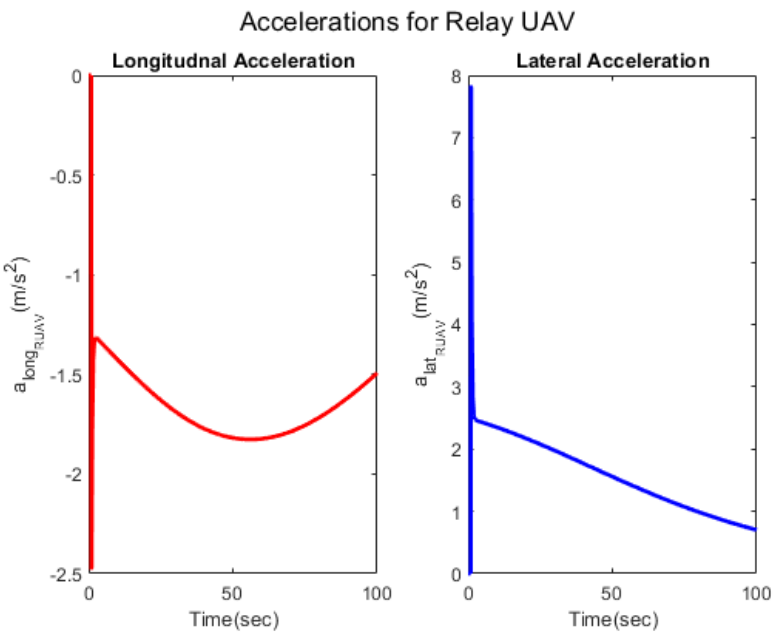

Figure 67 Longitudinal and Lateral Acceleration: RUAV

Figure 67 shows longitudinal and lateral acceleration for the R-UAV.

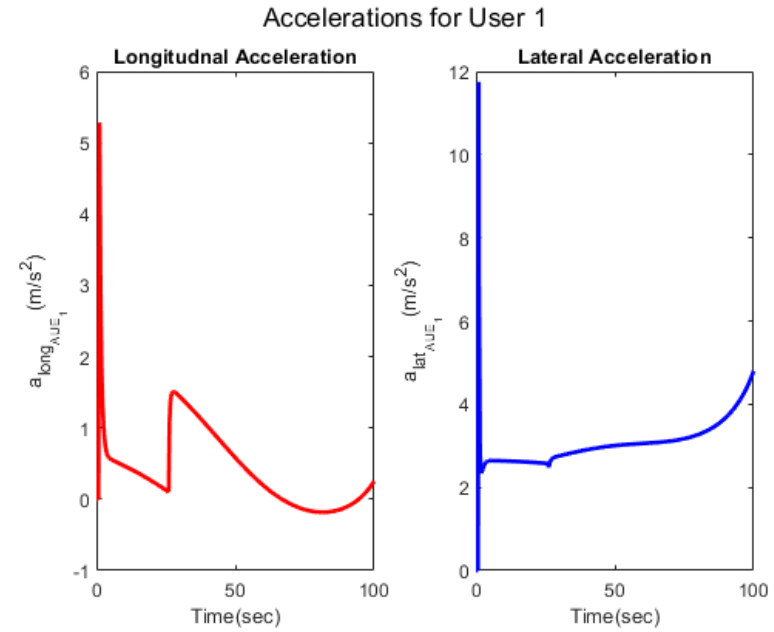

Figure 68 Longitudinal and Lateral Acceleration: UE1

Figure 68 shows longitudinal and lateral acceleration for the AUE1.

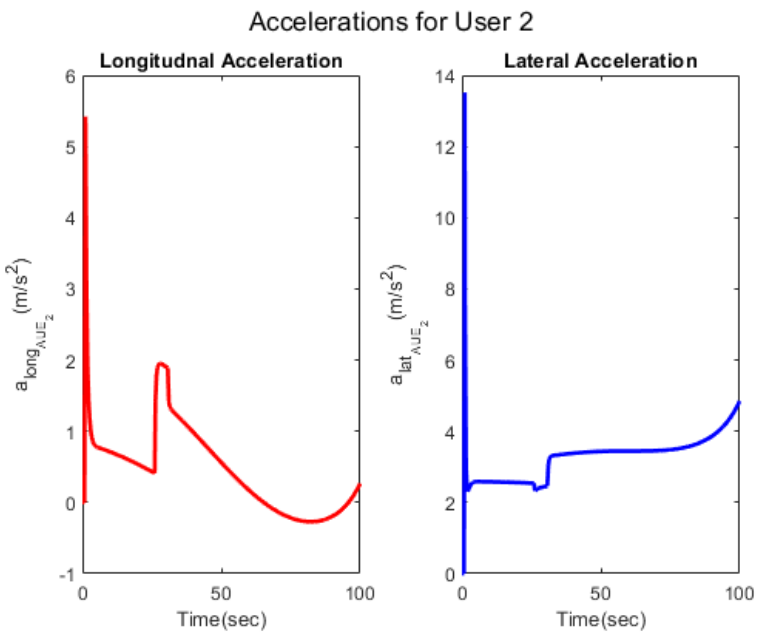

Figure 69 Longitudinal and Lateral Acceleration: UE2

Figure 69 shows longitudinal and lateral acceleration for the AUE2.

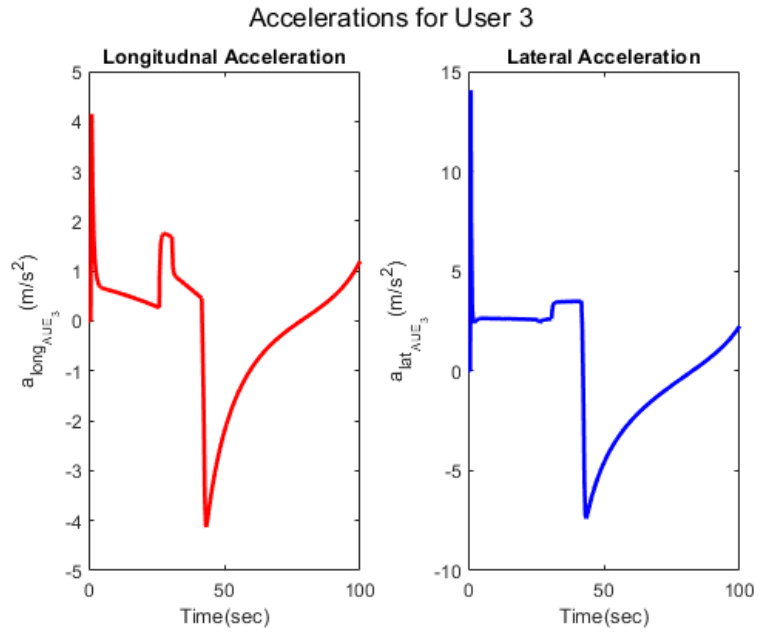

Figure 70 Longitudinal and Lateral Acceleration: UE3

Figure 70 shows longitudinal and lateral acceleration for the AUE3.

Chapter 5 Conclusions and Future Work

5.1 Conclusions

In this thesis, guidance laws to facilitate development of communication link between UAVs have been presented. These have been developed using the collision cone theory. The guidance laws governing the lateral and longitudinal acceleration of the UAVs present a well-defined methodology to guide the movement of UAVs using the relative position and velocity of the UAVs in the system.

These the guidance laws can create linked or collaborative teams of UAVs that can act as access points in dynamic communication networks, in areas where establishing full-fledged communication towers etc. might be an issue.Simulation results using MATLAB are presented.

Future work can include the introduction of an optimization framework to determine the guidance law gain, as well as extended to 3-D scenarios.

References

[1] Roser, M., Ritchie, H., & Ortiz-Ospina, E. (2021). Internet. Retrieved 10 October 2021, from https://ourworldindata.org/internet

[2] Gupta, L. & Jain, R. (2016) "Survey of Important Issues in UAV Communication Networks", *IEEE COMMUNICATIONS SURVEYS & TUTORIALS, VOL. 18, NO. 2 Retrieved from: IEEE Xplore*

[3] Baba, Y., Yamaguchi, M., & Howe, R. (1993). Generalized guidance law for collision courses. Journal Of Guidance, Control, And Dynamics, 16(3), 511-516. doi: 10.2514/3.21039

[4] Chakravarthy, Animesh & Ghose, Debasish. (1998). Obstacle avoidance in a dynamic environment: A collision cone approach. Systems, Man and Cybernetics, Part A: Systems and Humans, IEEE Transactions on. 28. 562 - 574. 10.1109/3468.709600.

[5] Coppola, M., McGuire, K.N., Scheper, K.Y.W. et al. On-board communication-based relative localization for collision avoidance in Micro Air Vehicle teams. Auton Robot 42, 1787–1805 (2018). https://doi.org/10.1007/s10514-018-9760-3

[6] Li, L., Chang, T., & Cai, S. (2020). UAV Positioning and Power Control for Two-Way Wireless Relaying. IEEE Transactions on Wireless Communications, 19(2), 1008-1024. doi: 10.1109/twc.2019.2950301

[7] Al-Hourani, A., Kandeepan, S., & Jamalipour, A. (2014). Modeling air-to-ground path loss for low altitude platforms in urban environments. 2014 IEEE Global Communications Conference. doi: 10.1109/glocom.2014.7037248

[8] Azari, M., Rosas, F., Chen, K., & Pollin, S. (2016). Optimal UAV Positioning for Terrestrial-Aerial Communication in Presence of Fading. 2016 IEEE Global Communications Conference (GLOBECOM). doi: 10.1109/glocom.2016.7842099

[9] Azari, M., Rosas, F., Chen, K., & Pollin, S. (2018). Ultra-Reliable UAV Communication Using Altitude and Cooperation Diversity. IEEE Transactions on Communications, 66(1), 330-344. doi: 10.1109/tcomm.2017.2746105

[10] Azari, M., Murillo, Y., Amin, O., Rosas, F., Alouini, M., & Pollin, S. (2017). Coverage maximization for a poisson field of drone cells. 2017 IEEE 28Th Annual International Symposium on Personal, Indoor, And Mobile Radio Communications (PIMRC). doi: 10.1109/pimrc.2017.8292753

[11] Azari, M., Rosas, F., Chen, K., & Pollin, S. (2016). Joint Sum-Rate and Power Gain Analysis of an Aerial Base Station. 2016 IEEE Globecom Workshops (GC Wkshps). doi: 10.1109/glocomw.2016.7848947.

[12] Guglielmo Marconi - Wikipedia. (2021). Retrieved 13 October 2021, from https://en.wikipedia.org/wiki/Guglielmo_Marconi#Radio_work

[13] Evolution of wireless technologies 1G to 5G in mobile communication - RF Page. (2021). Retrieved 12 October 2021, from https://www.rfpage.com/evolution-of-wireless-technologies-1g-to-5g-in-mobile-communication/

[14] Yan, C., Fu, L., Zhang, J., & Wang, J. (2019). A Comprehensive Survey on UAV Communication Channel Modeling. IEEE Access, 7, 107769-107792. doi: 10.1109/access.2019.2933173

[15] Signal-to-Noise Ratio (SNR) and Wireless Signal Strength - Cisco Meraki. (2021). Retrieved 16 October 2021, from https://documentation.meraki.com/MR/WiFi_Basics_and_Best_Practices/Signal-to-Noise_Ratio_(SNR)_and_Wireless_Signal_Strength

[16] What is Noise Floor » Electronics Notes. (2021). Retrieved 16 October 2021, from https://www.electronics-notes.com/articles/radio/radio-receiver-sensitivity/what-is-noise-floor.php

[17] Butler, J. (2013). Wireless networking in the developing world (p. 15). [S.l.]: Limehouse Book Sprint Team.

[18] When to Use 20mhz vs 40mhz vs 80mhz. (2019). Retrieved 16 October 2021, from https://www.cbtnuggets.com/blog/certifications/cisco/when-to-use-20mhz-vs-40mhz-vs-80mhz

[19] T-Mobile US. (2018). Retrieved 16 October 2021, from https://halberdbastion.com/intelligence/mobile-networks/t-mobile-us

[20] Johnson, R. (1984). Antenna Engineering Handbook (2nd ed.). New York, NY: McGraw-Hill, Inc. p. 1-12. ISBN 0-07-032291-0.

[21] Friis, H. (1946). A Note on a Simple Transmission Formula. Proceedings Of The IRE, 34(5), 254-256. doi: 10.1109/jrproc.1946.234568

[22] Atmel Corporation®, Application Note 9144C–RKE–07/15 “Range Calculation for 300MHz to 1000 MHz Communication Systems”, 2015.

[23] Abdi, A., Tepedelenlioglu, C., Kaveh, M., & Giannakis, G. (2001). On the estimation of the K parameter for the Rice fading distribution. IEEE Communications Letters, 5(3), 92-94. doi: 10.1109/4234.913150

[24] Tholen, K., Sunkara, V., Chakravarthy, A., & Ghose, D. (2018). Achieving Overlap of Multiple, Arbitrarily Shaped Footprints Using Rendezvous Cones. Journal Of Guidance, Control, And Dynamics, 41(6), 1290-1307. doi: 10.2514/1. g002932

[25] Chakravarthy, A., & Ghose, D. (2016). Guidance for Precision Three-Dimensional Maneuvers Through Orifices Using Safe-Passage Cones. Journal Of Guidance, Control, And Dynamics, 39(6), 1325-1341. doi: 10.2514/1. g001546